american physiological society

JNP JOURNAL OF NEUROPHYSIOLOGY

J Neurophysiol 134: 2047–2069, 2025.
First published November 6, 2025; doi:10.1152/jn.00621.2024

RESEARCH ARTICLE

Control of Movement

Changes in muscle synergy structure and activation patterns underlie force field adaptation, retention, and generalization

Michael Herzog,[1] Denise Jennifer Berger,[2,3] Marta Russo,[2,4] Andrea d'Avella,[2,5]* and Thorsten Stein[1]*

[1]*BioMotion Center, Institute of Sports and Sports Science, Karlsruhe Institute of Technology, Karlsruhe, Germany;* [2]*Laboratory of Neuromotor Physiology, IRCCS Fondazione Santa Lucia, Rome, Italy;* [3]*Department of Systems Medicine and Centre of Space Bio-Medicine, University of Rome Tor Vergata, Rome, Italy;* [4]*Institute of Cognitive Sciences and Technologies, National Research Council, Rome, Italy; and* [5]*Department of Biology, University of Rome Tor Vergata, Rome, Italy*

Abstract

Humans can adapt their motor commands in response to errors when they perform reaching movements in new dynamic conditions, a process called motor adaptation. They acquire knowledge about the new dynamics, which they can use when they are reexposed and, limitedly, generalize to untrained reaching directions. Although force field adaptation, retention, and generalization have been thoroughly investigated at a kinematic and kinetic task level, the underlying coordination at a muscular level remains unclear. Many studies propose that the central nervous system uses low-dimensional control, that is, coordinates muscles in functional groups: so-called muscle synergies. Accordingly, we hypothesized that changes in muscle synergy structure and activation patterns represent the acquired knowledge underlying force field adaptation, retention, and generalization. To test this, 36 male humans practiced reaching to a single target in a viscous force field and were tested for retention and generalization to new directions, while we simultaneously measured muscle activity from 13 upper-body muscles. We found that muscle synergies used for unperturbed reaching cannot explain the muscle patterns when adapted. Instead, muscle synergies specific to this adapted state were necessary, alongside a novel four-phasic pattern of muscle synergy activation. Furthermore, these structural changes and patterns were also evident during retention and generalization. Our results suggest that reaching in an environment with altered dynamics requires structural changes to muscle synergies compared with unperturbed reaching, and that these changes facilitate retention and generalization. These findings provide new insights into how the central nervous system coordinates the muscles underlying motor adaptation, retention, and generalization.

NEW & NOTEWORTHY Humans can adapt reaching movements to new dynamics, use the acquired knowledge when reexposed, and partly generalize it to new conditions. Although force field adaptation, retention, and spatial generalization have been thoroughly investigated at a kinematic and kinetic task level, the coordination of the underlying muscles remains elusive. We observed structural changes in muscle synergies—functionally coactivated muscles—with adaptation. These changes facilitated retention and spatial generalization. These findings provide new insights into motor adaptation.

coordination; force field adaptation; motor adaptation; motor learning; muscle synergies

INTRODUCTION

Humans can adapt their motor commands in response to errors when their reaching movements are perturbed, a process called motor adaptation (1). Furthermore, they can reuse the acquired knowledge when they are perturbed again and can partly generalize it to unpracticed reaching directions (2–7). Many studies have thoroughly analyzed force field adaptation, retention, and generalization at the level of task-related variables, describing and modeling the mapping of end-point kinematics and kinetics (8–11). However, how the central nervous system (CNS) coordinates motor adaptation at the

*A. d'Avella and T. Stein contributed equally to this work.
Correspondence: M. Herzog (michael.herzog@kit.edu).
Submitted 20 December 2024 / Revised 30 January 2025 / Accepted 31 October 2025

level of muscle activations has not been fully investigated. The CNS may implicitly represent acquired knowledge and generate motor commands by organizing muscle synergies (12–16). Through muscle synergies—coordinated recruitment of groups of muscles acting together as functional units—the CNS may control a small number of units rather than every muscle, thereby reducing the dimensionality of the control problem (13, 17, 18). Furthermore, by flexibly combining and sharing synergies, a large behavioral repertoire can be generated (14, 19–22).

To date, it remains unexplored how muscle synergies are related to force field adaptation, retention, and generalization, and what changes in their structure and activation patterns lead to the observed task-level kinematics and kinetics. Although isometric visuomotor rotation studies (23–25) showed that adaptation and spatial generalization do not require additional muscle synergies, a study by Oscari et al. (26) hints that force field adaptation does require additional synergies. Furthermore, studies with a few muscles' electromyograms (EMGs) in force field adaptation show two principal mechanisms. First, there is cocontraction of muscles acting around the elbow and shoulder joints, which decreases during adaptation but does not vanish completely (27–29). Second, the activity of specific muscles counteracting the force field increases, and their activation timing shifts toward the movement start (29–31). Furthermore, even after a plateau in kinematic- and kinetic-dependent variables, muscle activity continues to decrease, presumably to reduce effort (31, 32). Accordingly, adaptation may be represented either by a combination of baseline reaching muscle synergies or by specific, effort-optimized muscle synergies. Either way, if muscle synergies viably represent the coordination of force field adaptation at a muscular level, we expect them to also represent retention and spatial generalization. In particular, if muscle synergies change to accommodate specific requirements for adaptation to reaching in some directions, they are a poor choice for capturing muscle patterns in unpracticed reaching directions, in line with previous narrow spatial generalization findings (3, 4, 7).

To investigate how muscle synergies underlie force field adaptation, retention, and generalization at a muscular level, we first examined task-level variables. Accordingly, we hypothesized that (H_{Task} *1*) people adapt, deadapt, and readapt to the force field and that (H_{Task} *2*) spatial generalization decreases with distance from the practiced movement direction. Building on this, we then analyzed muscle activation patterns and hypothesized that ($H_{Synergies}$ *1*) the muscle patterns of force field adaptation can be reconstructed by a combination of baseline reaching synergies. As this hypothesis did not hold, we hypothesized that ($H_{Synergies}$ *2*) specific muscle synergies are required. Finally, we hypothesized that ($H_{Synergies}$ *3*) muscle synergies acquired through adaptation are only locally applicable, reflecting the narrow spatial generalization force field adaptation findings.

MATERIALS AND METHODS

Participants

Thirty-six right-handed male volunteers (age, 25.9 ± 2.8 yr; height, 1.80 ± 0.05 m; body weight, 77.2 ± 9.5 kg; handedness tested according to Ref. 33), naïve to force field adaptation experiments, provided written informed consent before participating. The Karlsruhe Institute of Technology Ethics Committee approved the study.

Apparatus and Task

The participants sat at a KINARM End-Point Lab with a virtual reality (VR) display (KINARM, Kingston, Canada, Fig. 1). The chair's height was individually adjusted so that the participant sat upright, leaning his forehead against the VR frame, and had a 90° angle between the upper and forearm. In the starting position, the handle was located on the mid-sagittal plane in front of the torso. The participants performed 15 cm center-out point-to-point movements in the horizontal plane with their right hand. The VR display showed the handle's position as well as the starting and target points, but obscured the view of the handle, hands, and arms. Participants were instructed to move the handle from the start to the target within 550 ± 50 ms after the handle had resided at the start point for at least 800 ms. The target color changed when reached, giving participants feedback on whether the specified movement time was met (green, within the time frame; blue, too fast; and red, too slow). After the handle remained within the target for 800 ms, the manipulandum moved it back to the start for the subsequent trial. The five targets were located at −90°, −45°, 0°, 45°, and 90° (Fig. 2).

Experimental Design

Trial conditions.

Three trial types were used: null field (NF), force field (FF), and error clamp (EC). In NF trials, the handle was freely movable without perturbing forces. In FF trials, a counterclockwise, velocity-dependent force field acted according to the formula:

Figure 1. Experimental setup. A participant with EMG electrodes attached sits at the KINARM End-Point Lab (KINARM, Kingston, Canada). EMG, electromyogram.

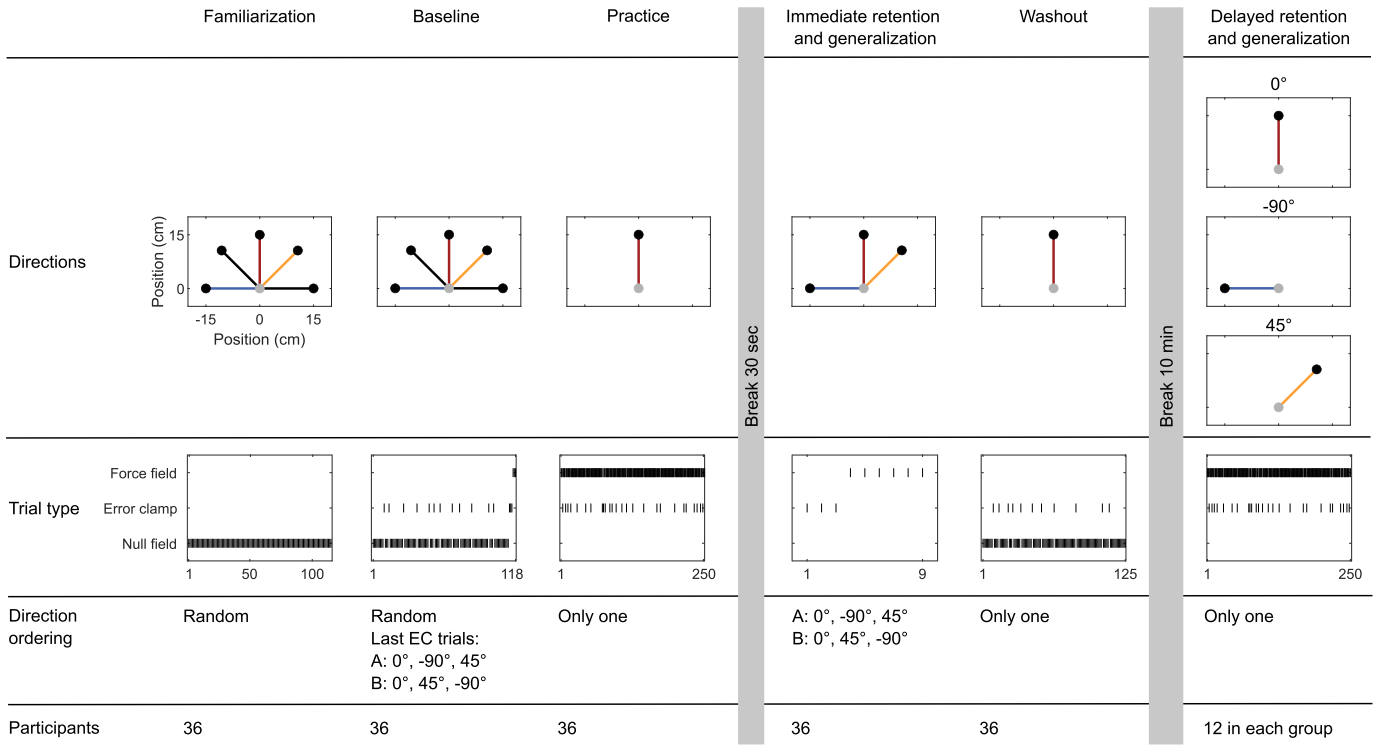

Figure 2. Experimental protocol. Participants performed center-out reaching movements of 15 cm in length. Start points are indicated by gray circular markers and target points by black circular markers. The top row shows the movement directions, and the second row shows the sequences of trial types. After washout, the 36 participants were randomly and evenly assigned to either the delayed retention, −90° generalization, or 45° generalization group. EC, error clamp.

$$\vec{F} = k \cdot \begin{pmatrix} \cos\theta & -\sin\theta \\ \sin\theta & \cos\theta \end{pmatrix} \cdot \begin{pmatrix} \dot{x} \\ \dot{y} \end{pmatrix},$$

with k being the force field magnitude fixed at 20 Ns/m. The angle θ was fixed at 90°. Therefore, the force field always steered the handle's movement orthogonally to its direction of motion. The handle's velocity components are given by $\begin{pmatrix} \dot{x} \\ \dot{y} \end{pmatrix}$. In EC trials, the End-Point Lab restricted the motion to a small channel connecting the start and end points (34, 35). Therefore, the manipulandum created virtual walls with a viscosity of 10 kNs/m and a stiffness of 1 kN/m.

Group assignment and schedule.

The schedule comprised six successive phases: familiarization, baseline, practice, immediate retention and generalization, washout, and delayed retention and generalization (Fig. 2). Participants accustomed themselves to the task during the familiarization phase, which consisted only of NF trials with the directions in a random order (same order for all participants). During baseline, they reached to each target 20 times without perturbing forces (NF trials) and three times in the EC condition in a random order. The last three trials were FF trials in the −90°, 0, and 45° directions. During practice, they performed 250 reaches in the FF condition to the 0° target. Therein, 26 EC trials were randomly interspersed. After a 30-s break, participants were tested for immediate retention (0° target) and generalization (−90° and 45° targets). For this purpose, the three targets were first reached in the EC condition with one trial per direction. Thereafter, the three targets were reached in the FF condition with two trials per direction. In both conditions, all participants first reached to the 0° target. After the 0° target, half of the participants reached to the −90° and then to the 45° target (*group A* in Fig. 2) and the other half first reached to the 45° and then to the −90° target accordingly (*group B* in Fig. 2). This was followed by the washout, comprising 125 trials (114 NF and 11 EC). After a 10-min break, the delayed retention and generalization phase followed. Every participant was randomly assigned to one of three groups (−90°, 0°, or 45°; each $N = 12$). The participants reached 250 times to one of the three targets only (target depending on group assignment) with perturbing forces. 26 EC trials were interspersed at the same trial number as during the practice phase. Participants could let go of the handle during the breaks.

Data Analysis

Kinematic (hand position and velocity) and kinetic (interaction forces) data measured at the manipulandum's handle were recorded at 1,000 Hz with KINARM Dexterit-E software (KINARM, Kingston, ON, Canada).

Thirteen surface EMG electrodes (4,000 Hz; Noraxon USA, Scottsdale, AZ) captured upper-body muscle activity of the following muscles (Fig. 1): trapezius (descending "TrapD," transverse "TrapT," and ascending "TrapA"), deltoid (anterior "DeltA," middle "DeltM," and posterior "DeltP"), latissimus dorsi ("LatDorsi"), pectoralis major ("PectMaj"), serratus anterior ("SerrA"), triceps brachii (lateralis "TriLat" and medialis "TriMed"), biceps brachii (long head, "Bic"), and brachioradialis ("Bra"). Participants' skin

was prepared by shaving, abrasion, and cleansing with alcohol to ensure good electrode-skin contact. Then, Ag/AgCl electrodes were attached according to SENIAM guidelines (36, 37).

Preprocessing.

Raw kinematic and kinetic data were filtered with a fourth-order Butterworth low-pass filter and a cut-off frequency of 6 Hz (kinematic) and 10 Hz (kinetic) following previous studies (38, 39). Movement start was defined as the instant the participant left the start point, and movement end was when he reached the target point for the first time. Raw EMG data were bandpass filtered with a 20–450 Hz, fourth-order zero-lag Butterworth filter (30). ECG artifacts apparent in the recordings of the trunk muscles were removed with a template-matching procedure (40). Subsequently, 50 Hz noise was removed with a second-order zero-lag Butterworth notch filter [50 Hz and harmonics up to 500 Hz (41, 42)]. The filtered EMG data were full-wave rectified and envelopes were calculated using a fourth-order zero-lag Butterworth low-pass filter with a cut-off frequency of 10 Hz. EMG data were segmented from 200 ms before the participant left the start point until 200 ms after they reached the target for the first time, for example, including potential overshooting corrections. The segmented data were time-normalized to 101 time points. Then, the data were amplitude-normalized per muscle and participant to the maximum activity across all trials. Finally, the tonic EMG component was removed from all trials (43). To do so, a linear ramp was modeled using the average EMG envelope of each muscle in the 200 ms before the movement started and the 200 ms after the target was reached. Each calculation of averages included all baseline trials in the same direction. This direction-, muscle-, and participant-specific estimation of the tonic component was then subtracted from all respective trials. The remaining phasic parts of the EMG could contain negative values, which were clipped to zero. After careful observation, TrapD was excluded as it contributed only noise. No other muscles, trials, or participants were excluded. All processing and analysis steps were performed in MATLAB (RRID:SCR 001622, R2023b, Natick, MA).

Kinematic and kinetic dependent variables.

Following previous studies, adaptation was assessed with a kinematic and a kinetic measure (44, 45). The kinematic variable PD_{max} quantifies the maximum perpendicular distance between a trial's trajectory and a virtual straight line connecting the start and target. Although it quantifies the net motor output with all control processes involved (39), the kinetic force field compensation factor (FFCF) quantifies the participant's force field prediction (34, 35). FFCF was calculated by linear regression according to the formula:

$$F_{actual}(t) = a_1 \cdot F_{ideal}(t) + a_0 + e(t),$$

where the error $e(t)$ was minimized (least-squares). The regression coefficient a_0 was the axis intercept, and a_1 was the slope. The slope serves as FFCF. F_{acutal} was the force with which the participant pressed the handle against the virtual wall. F_{ideal} was the product of the force field matrix and the trial's velocity profile, resulting in the force profile with which the participant would have produced a straight trajectory in the force field. If F_{ideal} and F_{actual} are identical, the FFCF is 1; if unrelated, the FFCF is 0. To consider only changes based on adaptation and generalization, all PD_{max} and FFCF values were participant- and target-specific baseline-subtracted (46).

Extraction and fitting of muscle synergies.

We set up three hypotheses to investigate how force field adaptation, retention, and spatial generalization are represented in a modular structure, using the following "extract-and-fit" approach (Fig. 3). To test $H_{Synergies}$ *1*, that the muscle patterns of force field adaptation can be reconstructed by a combination of baseline reaching synergies, we extracted muscle synergies from the baseline trials (see *Extraction of baseline muscle synergies*) and tested their ability to explain the muscle patterns of the adapted state by fitting them on adapted state trials (see *Quality of reconstruction of adapted state data with baseline muscle synergies*). A bad reconstruction quality would indicate that baseline muscle synergies do not suffice to explain the muscle pattern used by the participants in the adapted state.

This leaves two possibilities: either the baseline synergies are part of a larger set of synergies, which also includes the adapted state-specific synergies, or both the baseline and adapted state-specific synergies include synergies distinct for each set, that is, coming from sets of synergies, which are nonintersecting ($H_{Synergies}$ *2*). To test this, we compare a pooled (W-POOL) to a shared-and-specific (W-SAS) muscle synergies extraction (see *Fitting of the pooled and the shared-and-specific muscle synergy extraction to the adapted state*). In brief, for a pooled extraction, the input comprises the baseline and the adapted state muscle pattern, assuming a common basis. The shared-and-specific extraction is an approach that compares subspace dimensions and accounts for noise (see *Extraction of shared-and-specific muscle synergies of baseline and the adapted state*). Muscle synergies are thought to span low-dimensional subspaces in the muscle space. Although a subspace is unique, its basis vectors (muscle synergies) are ambiguous. Due to limited data available or noise, baseline and adapted state muscle synergies may therefore differ, despite that the subspaces they each span are the same (47, 48). Accordingly, to disentangle shared and specific subspace dimensions, we use a shared-and-specific muscle synergy extraction approach. In other words, the approach aims to best identify the intersecting (i.e., shared) and the disjunct (i.e., specific) parts of the two subspaces spanned by two sets of muscle synergies (47, 49). Another alternative to the shared-and-specific extraction would be separate extractions with a subsequent similarity analysis. However, this may be misleading as the similarity depends on the single set's muscle synergy extraction (48). Due to limited data availability, any two distinct synergies of one dataset could be extracted as a single (merged) synergy, which may decrease the similarity value when comparing with a synergy from the second dataset. Hence, this approach may underestimate the shared features of two datasets (47).

Finally, to test $H_{Synergies}$ *3*, that muscle synergies acquired through adaptation are only locally applicable, reflecting the narrow spatial generalization force field adaptation findings, we took two steps. First, we wanted to know whether the

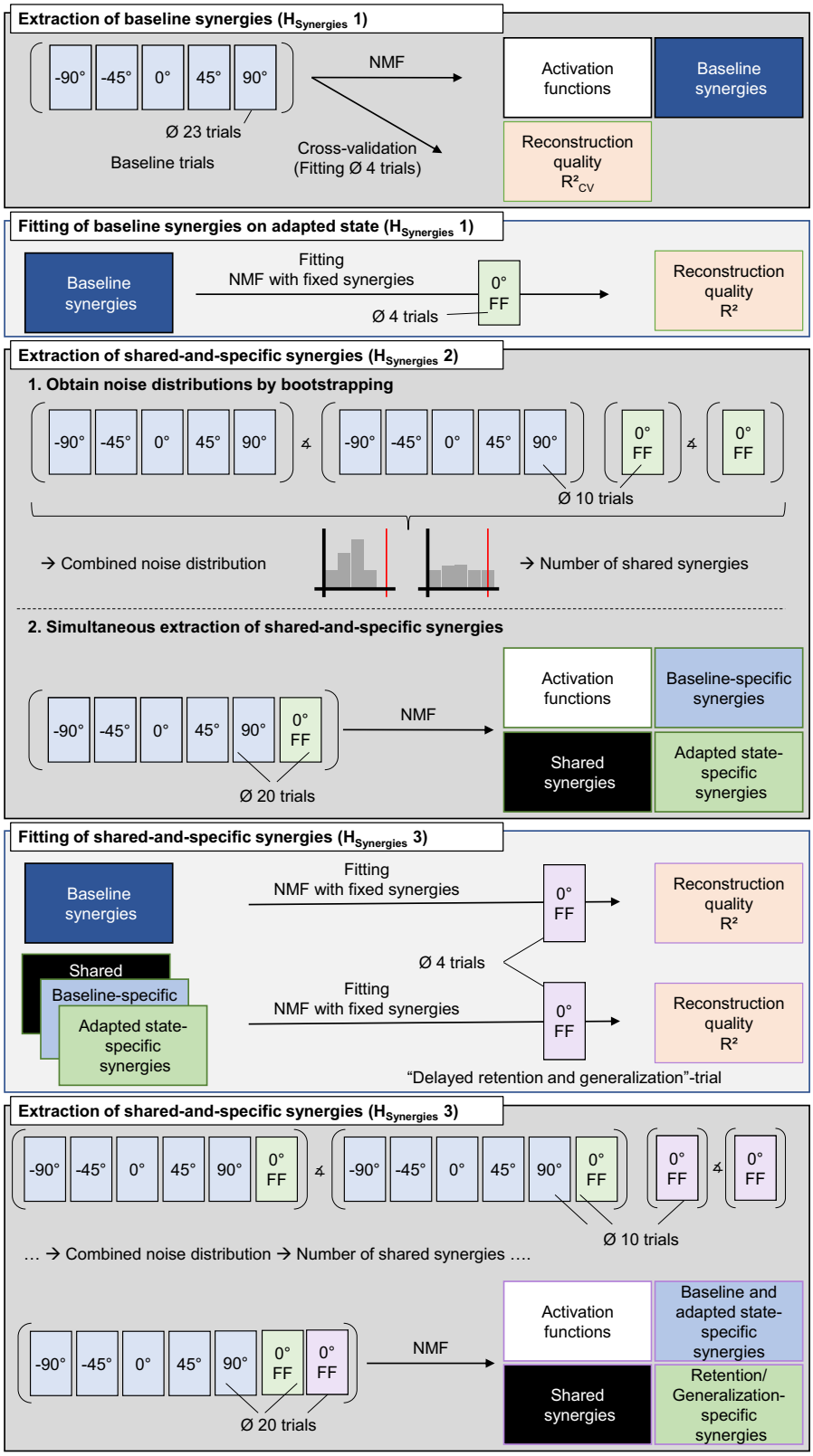

Figure 3. Summary of muscle synergy analyses. We followed an iterative "extract-and-fit" approach. First, baseline synergies were extracted and fitted to the adapted state. Next, shared-and-specific synergies of the baseline and adapted state were extracted and fitted to the first delayed retention/generalization trials. Finally, shared-and-specific synergies were extracted from the baseline and adapted state together and the first delayed retention/generalization trials. The ∡ symbol illustrates the calculated principal angle. FF, force field; NMF, non-negative matrix factorization.

muscle synergies that capture not only baseline muscle patterns but also those of the adapted state—the acquired knowledge through adaptation—can account for retention and generalization. Hence, we fitted separately *1*) the shared-and-specific muscle synergies and *2*) the baseline synergies to the delayed retention/generalization trials (averaged in blocks of four FF). We then compared the reconstruction qualities of *1*) and *2*). If the reconstruction quality of *1*) was significantly better, this would indicate that the acquired knowledge through adaptation facilitates retention and

generalization (see *Fitting shared-and-specific muscle synergies of baseline and the adapted state to the trials of the delayed retention and generalization phase*). Second, we extracted shared-and-specific synergies from the baseline and the adapted state together and the first 20 delayed retention/generalization FF trials (see *Extraction of shared-and-specific muscle synergies of the baseline and the adapted state together, and the start of the delayed retention and generalization phase*), intending to identify a muscle synergy representation of what facilitates delayed retention and generalization.

Extraction of baseline muscle synergies. For every participant, a matrix $\mathbf{EMG} \in \mathbb{R}_{\geq 0}^{12\times 101\cdot 5}$ was composed, with the EMG data of the 12 muscles in rows and the five averaged trials with 101 time points each in columns. Each averaged trial comprises the averaged EMG data of the 23 baseline trials to the same target. We extracted spatial muscle synergies with non-negative matrix factorization [NMF (50–52)]. NMF reduces the dimensionality of the EMG dataset by approximating it with N trial-invariant spatial muscle synergies $\boldsymbol{W_n} \in \mathbb{R}_{\geq 0}^{12\times 1}$, vectors specifying relative muscle activation levels, as well as N synergy activation profiles $\boldsymbol{C_n} \in \mathbb{R}_{\geq 0}^{1\times 101}$:

$$\mathbf{EMG}(t) = \sum\nolimits_{n\in N} \boldsymbol{W_n} \cdot \boldsymbol{C_n}(t).$$

The decomposition was repeated 50 times with random initial conditions to avoid convergence to local minima and was limited to 3,000 iterations (53, 54). The reconstruction quality was assessed using the multivariate $R^2 = 1 - \mathrm{SSE/SST}$. SSE was calculated as the sum of the squared residuals, and SST as the sum of the squared residuals from the mean vector (43). The number of extracted synergies N was chosen at the R^2 knee point, after which the R^2 curve remained approximately straight. The R^2 knee point was calculated using a series of linear regressions fitted to the R^2 versus N curve (MATLAB `polyfit`), beginning with a regression across the interval [1, 12]. We then iteratively excluded the smallest value from the regression interval. We identified the optimal number of synergies N as the first N with a regression line from N to 12 with a mean square error smaller than 10^{-4} (43).

Quality of reconstruction of adapted state data with baseline muscle synergies. To investigate whether baseline reaching muscle synergies can reconstruct the muscle patterns of force field adaptation ($H_{Synergies\ 1}$), they were tested for their ability to explain the muscle patterns (R^2) in the adapted state. In particular, NMF was applied to the averaged EMG data from the last four force field trials of the adaptation phase, keeping the baseline synergies ($\boldsymbol{W_n} \in \mathbb{R}_{\geq 0}^{12\times 1}$) fixed and updating only the activation profiles ($\boldsymbol{C_n} \in \mathbb{R}_{\geq 0}^{1\times 101}$). Then, we compared the R^2 values of the reconstruction with a cross-validated R^2_{CV} of the baseline extraction. Therefore, we repeated the following process 100 times. Four randomly selected baseline trials to the same direction were averaged and constituted the test part of the cross validation. The remaining 19 trials were averaged and horizontally concatenated with the remaining four average baseline trials, constituting the training part of the cross validation (see *Extraction of baseline muscle synergies*). Muscle synergies were extracted from the training part and fitted to the test part. Cross validation was used to prevent a misleading overestimation of the synergies' reconstruction ability on the baseline phase (55).

Extraction of shared-and-specific muscle synergies of baseline and the adapted state. To investigate whether specific muscle synergies are required for force field adaptation ($H_{Synergies\ 2}$), we extracted three sets of synergies from the combined baseline and adapted state data: one set shared between baseline and adapted state data, a second set specific to the baseline data, and a third set specific to the adapted state data (47, 49). We determined the number of shared synergies as the dimension of the shared subspace spanned by the synergies extracted separately from baseline and adapted state. To estimate such a dimension, we used a bootstrapping procedure that differentiated noise and structural differences (56, 57). This procedure assumes that differences in the synergies extracted from different subsets of trials in the same conditions are due to noise rather than structural differences.

The procedure comprised four steps. First, muscle synergies were extracted from the baseline and adapted state separately following the description in *Extraction of baseline muscle synergies*. Thereby, the EMG data matrix of the baseline state comprised the 12 muscles in rows and the five averaged trials in columns. Each trial was the average of the 20 NF baseline trials to the same direction. The adapted state matrix comprised 12 muscles in rows and one averaged trial over the last 20 FF. The principal angles between the subspaces spanned by the two sets of muscle synergies were calculated [$\theta_{\text{Baseline vs. adapted state}}$ (58)]. Second, both baseline and adapted state datasets were split into two disjunct, equal-sized subdatasets. The two baseline subdatasets comprised five averaged trials, each from 10 randomly selected trials in the same direction. The two adapted state subdatasets constituted one averaged trial, calculated on 10 randomly selected trials of the last 20 FF trials during adaptation. Muscle synergies were extracted from each subset, and the principal angles between the subspaces spanned by the muscle synergies of the same phase were calculated. The second step was repeated 500 times, each time with a random drawing with replacement of trials included in the subsets. This resulted in two principal angle distributions, one for the baseline and one for the adapted state. These distributions quantify the noise inherent in the baseline and the adapted state data. Third, the principal angles from each subset were used to obtain a new distribution of principal angles between baseline and adapted state synergies due only to noise. To do so, two new subspaces representing the "noise subspaces" for the baseline and adapted state were calculated starting from a common base and rotating each subspace according to the respective principal angle distribution. Then, the principal angles between the two newly constructed "noise subspaces" of the baseline and adapted state were calculated. The third step was repeated 500 times, providing a distribution of the principal angles from the "noise subspaces." Fourth, the latter distribution's 95th percentile (θ_{95}) was calculated and compared with the principal angles between the original baseline and original adapted state synergies (step one, $\theta_{\text{Baseline vs. adapted state}}$). The number of shared synergies was defined as the number of principal angles between the baseline and the adapted state, which were smaller than the

corresponding θ_{95}. This is based on the assumption that structural differences between muscle synergies are represented by much larger principal angles than those due to noise.

After these steps, which resulted in the number of muscle synergies shared between the baseline and adapted state, shared-and-specific muscle synergies were simultaneously extracted with an iterative process. The horizontal concatenation of the baseline and adapted state datasets, as described in the first step, constituted the input matrix for the NMF algorithm. Starting with the number of shared synergies, muscle synergies were extracted. The reconstruction qualities R^2_{Baseline} and $R^2_{\text{Adapted state}}$ were calculated and compared with the original R^2 values obtained during the first step of the shared extraction. If the original R^2 values were not reached, a new NMF decomposition was performed with the number of shared synergies plus one or two, depending on the R^2 comparisons. In addition, the matrix **C** with the synergy activation profiles was provided. **C** was initialized with random values in the cells for the shared synergies, baseline-, and adapted state-specific synergies to extract. The remaining cells were filled with zeros. Therefore, using the properties of the NMF multiplicative update rule, activation profiles specific to one phase were not considered for the other phase.

Fitting of the pooled and the shared-and-specific muscle synergy extraction to the adapted state. To disentangle whether the baseline synergies are part of a larger set of synergies, which also includes the adapted state-specific synergies, or both the baseline and adapted state-specific synergies include synergies distinct for each set, that is, coming from sets of synergies, which are nonintersecting ($H_{Synergies}$ *2*), we compared the pooled with the shared-and-specific extraction regarding their ability to reconstruct the muscle patterns of the adapted state.

First, we extracted muscle synergies from the pooled baseline and adapted state data, denoted by W-POOL. For the pooled extraction, the EMG data matrices of the baseline and adapted state were horizontally concatenated. The baseline part comprised the 12 muscles in rows and the five averaged trials in columns. Each trial was the average of the 20 NF baseline trials in the same direction. The adapted state part comprised 12 muscles in rows and one averaged trial over the last 20 to the last four FF trials, thus leaving out the last four FF trials. The average of the last four FF trials was used as the trial to which the pooled and shared-and-specific muscle synergies were fitted for comparison.

Second, we extracted shared-and-specific muscle synergies simultaneously, given the same dataset as for the pooled extraction and the information on the number of shared, baseline-specific, and adapted state-specific synergies obtained from the previous extraction (see *Extraction of shared-and-specific muscle synergies of baseline and the adapted state*), denoted by W-SAS.

Third, we fitted W-POOL and W-SAS to the muscle patterns of the adapted state trial, and compared the reconstruction qualities of the two fits, denoted by $R^2_{\text{W-POOL}\rightarrow\text{Adapted state}}$ and $R^2_{\text{W-SAS}\rightarrow\text{Adapted state}}$, respectively, by keeping the number of synergies equal between the two extractions. This is because both the pooled and the shared-and-specific approach will yield subspaces spanned by the extracted muscle synergies, so that baseline and adapted state-specific muscle patterns are within their subspaces. However, assuming specific and distinct adapted state synergies are necessary, the reconstructions (fits) of the muscle patterns of the adapted state will be different. The distinction can be made based on the dimensions of the subspaces: For a "fair" comparison, the number of synergies used for the fitting needs to be kept the same, as the reconstruction quality R^2 depends on the number of synergies. If $H_{Synergies}$ *2* is true (i.e., specific synergies are required), given that $H_{Synergies}$ *1* is false (i.e., baseline reaching muscle synergies cannot reconstruct the muscle patterns of force field adaptation), we expect the reconstruction quality $R^2_{\text{W-POOL}}$ to be lower than $R^2_{\text{W-SAS}}$ for the reconstruction of both the baseline and adapted state muscle patterns with the same number of synergies. As we have already established a procedure to determine the number of W-SAS, the number of W-POOL to use for the reconstruction of the baseline and adapted state muscle patterns must be equal to the sum of the number of shared and baseline-specific muscle synergies for the baseline and the number of shared and adapted state-specific muscle synergies for the adapted state.

Given that $H_{Synergies}$ *1* is false and *1*) $H_{Synergies}$ *2* is true, that is, adapted state-specific synergies are required, then the muscle patterns of the adapted state are generated by a set of muscle synergies distinct from the baseline synergies. With regard to the reconstruction quality, this means:

1a) $R^2_{\text{W-POOL}\rightarrow\text{Baseline}} < R^2_{\text{W-SAS}\rightarrow\text{Baseline}}$. This is because the reconstruction of the pooled dataset requires more synergies than the reconstruction of the baseline alone, and forcing the extraction to the number of W-SAS synergies makes W-POOL suboptimal.

1b) $R^2_{\text{W-POOL}\rightarrow\text{Adapted state}} < R^2_{\text{W-SAS}\rightarrow\text{Adapted state}}$, for the same reasons.

Given that $H_{Synergies}$ *1* is false and *2*) $H_{Synergies}$ *2* is false, that is, adapted state-specific synergies are not required, but a larger set of muscle synergies than baseline synergies alone. With regard to the reconstruction quality, this means:

2a) $R^2_{\text{W-POOL}\rightarrow\text{Baseline}} < R^2_{\text{W-SAS}\rightarrow\text{Baseline}}$. This is because W-POOL are optimized to explain both baseline and adapted state muscle patterns. As the number of synergies used for the fit is limited to the sum of shared and baseline-specific muscle synergies for the baseline, which is less than the number of W-POOL synergies, the baseline muscle patterns are less well captured.

2b) $R^2_{\text{W-POOL}\rightarrow\text{Adapted state}}$ not different from $R^2_{\text{W-SAS}\rightarrow\text{Adapted state}}$. The number of W-POOL synergies for the fit is equal to the sum of the shared and adapted state-specific muscle synergies, that is, the same number and so the same dimension is given, as the number is equal to the sum of the baseline and the additionally required synergies used for the pooled extraction.

Hence, the critical test was whether *1b*) or *2b*) is true.

Fitting shared-and-specific muscle synergies of baseline and the adapted state to the trials of the delayed retention and generalization phase. To test $H_{Synergies}$ *3*, that muscle synergies acquired through adaptation are only locally applicable, reflecting the narrow spatial generalization force field adaptation findings, we fitted *1*) the baseline

synergies and *2*) the shared-and-specific muscle synergies extracted from baseline and the adapted state (see *Extraction of shared-and-specific muscle synergies of baseline and the adapted state*) to blocks of four averaged FF trials of the delayed retention and generalization phase. Furthermore, we tested statistically their ability to reconstruct the muscle pattern (R^2) of the average of the first four FF trials in the delayed retention and generalization phase, as described below under *Muscle synergy analyses* in *Statistical Analysis*. If $H_{Synergies\ 3}$ holds, then the reconstruction using the shared-and-specific synergies compared with using baseline synergies would be best for the 0° group (retention), higher than zero for the 45° group (limited generalization), and zero for the −90° group (no generalization).

Extraction of shared-and-specific muscle synergies of the baseline and the adapted state together, and the start of the delayed retention and generalization phase. With a similar approach to the four steps described in *Extraction of shared-and-specific muscle synergies of baseline and the adapted state*, we extracted shared-and-specific synergies from the baseline and adapted state together, and the first 20 FF delayed retention/generalization trials. The aim was to identify a muscle synergy representation of what facilitates retention and generalization. For the EMG data matrix of the baseline and adapted state, the same baseline matrix as described in *Extraction of shared-and-specific muscle synergies of baseline and the adapted state* was concatenated horizontally with one averaged trial over the last 20 FF trials during adaptation. For the EMG data matrix of the retention/generalization trials, the first 20 FF trials during this phase were averaged. We then calculated the noise distributions in a similar way as described in *Extraction of shared-and-specific muscle synergies of baseline and the adapted state*, with subsets of 10 averaged trials. We ensured that the muscle synergies extracted from the baseline and adapted state kept their structure as extracted in *Extraction of shared-and-specific muscle synergies of baseline and the adapted state*, that is, their number of shared and specific synergies. Therefore, we initialized the **C** matrix with random numbers in cells according to the shared-and-specific synergies and zeros otherwise. Hence, in these calculations, the synergy vectors' values and the activation functions' values could vary, but the general structure of the synergy extraction remained. The combined shared-and-specific extraction in the last step also used a specific initialization of the **C** matrix. **C** was initialized with random values in the cells for the shared-and-specific synergies between the baseline and adapted state together, and the first 20 delayed retention/generalization trials, and zeros otherwise.

Clustering of similar muscle synergies. To compare synergies extracted from different participants, we grouped them using cluster analysis. Each synergy was normalized to the maximum of its elements. First, hierarchical clustering [MATLAB `pdist` (Minkowski distance; $p = 3$), `linkage` (Ward option), and (59)] was used to determine the optimal number of clusters. The number was chosen by assessing *1*) the scree plot, which plots the within-cluster sum of squares of the linkage distance against the number of clusters, and *2*) the silhouette method (MATLAB `silhouette`), which quantifies the similarity of a given synergy to the other synergies in its cluster with respect to synergies from other clusters. The silhouette value s_{syn} for the synergy syn is calculated as follows:

$$s_{syn} = \frac{(b_{syn} - a_{syn})}{\max(a_{syn}, b_{syn})}.$$

Here, a_{syn} is the average distance (cosine similarity) from syn to the other synergies of the same cluster, and b_{syn} is the minimum average distance (cosine similarity) from syn to the synergies in a different cluster, minimized over the clusters. Silhouette values range from −1 to 1, with higher values indicating a better similarity. The number of clusters was chosen at the knee point of the scree plot and increased when a cluster contained low negative values (less than −0.3).

Second, the synergies were clustered with k-means++ based on their cosine similarity. The centroids are the synergies with the least distance (1 − cosine) to all synergies within one cluster (57).

Cosine tuning of the baseline synergy clusters.

Synergy tuning curves were calculated for each synergy cluster by a cosine fit using the integral under the mean activation of each synergy cluster and the target position [−90°, −45°, 0°, 45°, 90° (43)]. Therefore, the integrals were fitted with a linear regression according to the following formula (MATLAB `regress`):

$$\mathrm{act}(\theta) = \beta_0 + \beta_x \cos(\theta) + \beta_y \sin(\theta),$$

where act(θ) is the integral under the mean activation of each synergy cluster toward the target in the direction of θ. Synergies can be used to decelerate a movement going in the direction opposite to its "acting direction." Therefore, synergy tuning curves were calculated for the first 25% of the movement duration, ensuring tuning only to the "acting direction." The quality of the fits was assessed using R^2, and the significance of the cosine tuning was assumed when the P value of the regression between the data and the optimal cosine tuning was smaller than 0.05.

Statistical Analysis

Kinematic and kinetic dependent variables.

Differences in the kinematic and kinetic dependent variables, PD_{max} and FFCF, were tested as follows. Normality was assessed with the Shapiro–Wilk, the homogeneity of variances with Levene's, and the sphericity with the Mauchly tests. If the latter was violated, the Greenhouse-Geisser adjustment was used.

Whether the participants adapted and washed out ($H_{Task\ 1}$) was tested separately with dependent t tests comparing the means of the first two and last two FF trials and the first and last EC trials, respectively.

The immediate retention and generalization ($H_{Task\ 2}$) were assessed as follows: first, a one-way repeated-measurements ANOVA with subsequent post hoc t tests identified differences between the three groups (−90°, 0°, and 45°) on the PD_{max}-mean of the two FF trials. Second, the FFCF values were tested for differences against zero (0 = no retention/generalization) with one-sample t tests separately for each direction. Third, FFCF differences between the groups were tested with a one-way repeated-measurements ANOVA with subsequent post hoc t tests.

To determine whether people (re)adapt in the delayed retention and generalization phase, the three groups were tested separately with dependent t tests on *1*) the first and last two FF trials (PD_{max}) and *2*) the first and last EC trials (FFCF). Furthermore, the first FFCF values were tested for differences against zero (0 = no retention/generalization) with one-sample t tests to assess retention and generalization.

To investigate H_{Task} *2*, that generalization decreases with distance from the practiced movement direction, a linear mixed model (LMM) was used (MATLAB `fitlme`). LMM allows the consideration of repeated measures (*level 1*) of a single participant (*level 2*), instead of the required aggregation of data as in t tests or ANOVAs, which suits an adaptation experiment featuring intertrial changes. The group assignment was included as a dummy variable using reference coding (either DIR90 or DIR45 set to 1, or both to 0 for the DIR0 group). The first LMM was calculated with DIR0 as the reference group, and the second LMM with DIR90 as the reference group, allowing investigation of all pairwise comparisons. A random slope for the participant did not improve the model fit based on the change in the −2 log-likelihood and Akaike's information criterion [MATLAB's `linearmixedmodel.compare` function (60, 61)]. The residual plots were inspected to assess linearity and homoscedasticity as prerequisites for LMM, and no gross violations were found (62).

The LMM regression formula was:

$$\begin{aligned}\text{Adaptation}_{tp} = (\gamma_0 + u_{0p}) &+ \gamma_1\text{DIR90}_{tp} + \gamma_2\text{DIR45}_{tp} \\ &+ \gamma_3\text{TrialNumber}_{tp} \\ &+ \gamma_4\text{DIR90\_TrialNumber}_{tp} \\ &+ \gamma_5\text{DIR45\_TrialNumber}_{tp} + \epsilon_{tp}\end{aligned}$$

where Adaptation_{tp} represents the PD_{max} or FFCF value of the tth trial for the pth participant. The variable u_{0p} is a participant-specific random component, and the γs are fixed effect parameters for the group assignment (reference coding), trial number, and the interaction of trial number and group assignment. Accordingly, the following formula was used for the function specification of the `fitlme` function: Adaptation ~ (DIR90 + DIR45) × TrialNumber + (1 | Participant). The LMM was implemented using the maximum likelihood method. Twenty trials were included (16 for the PD_{max} LMM and 4 for the FFCF LMM).

Muscle synergy analyses.

A dependent t test was used to determine differences in the reconstruction quality of the baseline muscle synergies (R^2_{CV}) and their fit to the adapted state ($H_{Synergies}$ *1*; *Quality of reconstruction of adapted state data with baseline muscle synergies*). A dependent t test was used to determine differences in the reconstruction quality of the fit of W-POOL and W-SAS to the adapted state ($R^2_{\text{W-POOL}\rightarrow\text{Adapted state}}$ versus $R^2_{\text{W-SAS}\rightarrow\text{Adapted state}}$; $H_{Synergies}$ *2*; *Fitting of the pooled and the shared-and-specific muscle synergy extraction to the adapted state*). The Kruskal–Wallis and Wilcoxon tests were used to test for improvements in the reconstruction quality between fitting the baseline synergies and fitting the shared-and-specific synergies on the retention/generalization trials, as the distribution was not normal ($H_{Synergies}$ *3*).

General procedure.

For all statistics, the significance level (two-tailed) was set a priori at 0.05. It was adjusted for multiple comparisons post hoc with the Holm-Bonferroni correction (63) and to 0.025 for the LMM statistics, as the test was carried out with two reference groups. The effect sizes were determined with η^2_p and Cohen's $|d|$; and classified as small ($\eta^2_p \geq 0.01$, $|d| \geq 0.2$), medium ($\eta^2_p \geq 0.06$, $|d| \geq 0.5$), and large [$\eta^2_p \geq 0.14$, $|d| \geq 0.8$ (64)].

RESULTS

We were interested in how muscle synergies reflect force field adaptation, retention, and generalization at a muscular level. Therefore, we first examined whether all participants adapted, washed out, and showed retention/generalization (H_{Task} *1* and H_{Task} *2*; Fig. 4) based on the kinematic and kinetic dependent variables (PD_{max} and FFCF). Then, we examined the underlying muscle synergies of adaptation, retention, and generalization ($H_{Synergies}$ *1–3*).

Participants Adapted to the Force Field and Washed Out Successfully

When first exposed to the force field, participants' trajectories became typically curved and then, with practice, became almost straight again [PD_{max}: $t(35) = 14.03$, $P < 0.001$, $d = 2.86$; FFCF: $t(35) = -9.15$, $P < 0.001$, $d = -2.28$; Fig. 4, Supplemental Fig. S1]. Therefore, we can state that participants adapted to the force field. At the beginning of the washout, participants' trajectories became curved again, mirroring the initial trajectories of the adaptation phase, and then became almost straight again [PD_{max}: $t(35) = 22.60$, $P < 0.001$, $d = 5.15$; FFCF: $t(35) = -9.15$, $P < 0.001$, $d = -2.30$]. Hence, participants washed out. We therefore accept H_{Task} *1*, that the participants adapt to the force field and deadapt after its removal.

Participants Generalized Better to the 45° than to the −90° Target at the Immediate Retention and Generalization Test

After the adaptation period, all participants were tested for retention and generalization to the −90° and 45° targets. The ANOVA [$F(2, 58.01) = 216.45$, $P < 0.001$, $\eta^2_p = 0.86$] and post hoc t tests on the PD_{max} values revealed no difference between the 0° and the 45° target [$t(35) = -1.59$, $P = 0.120$, $d = -0.28$] but indicated that there were differences between 0° and −90° [$t(35) = 8.79$, $P < 0.001$, $d = 1.58$] as well as between the −90° and 45° targets [$t(35) = 8.22$, $P < 0.001$, $d = 1.56$]. Hence, the generalization to the 45° was not worse than the 0° retention, and better than the generalization to the −90° target.

The FFCF values were significantly different from zero for the 0° [$t(35) = 10.77$, $P < 0.001$, $d = 1.76$] and 45° target [$t(35) = 12.91$, $P < 0.001$, $d = 2.11$] but not the −90° target [$t(35) = 1.84$, $P = 0.075$, $d = 0.30$], indicating retention (0° target) and generalization to the 45° target only. The ANOVA [$F(2, 50.32) = 53.37$, $P < 0.001$, $\eta^2_p = 0.60$] and post hoc t tests on the FFCF values showed the best performance for retention, and better performance (i.e., better generalization) for the 45° than for the −90° target [−90° vs. 0°: $t(35) = -8.86$, $P < 0.001$, $d = -2.15$; −90° vs. 45°:

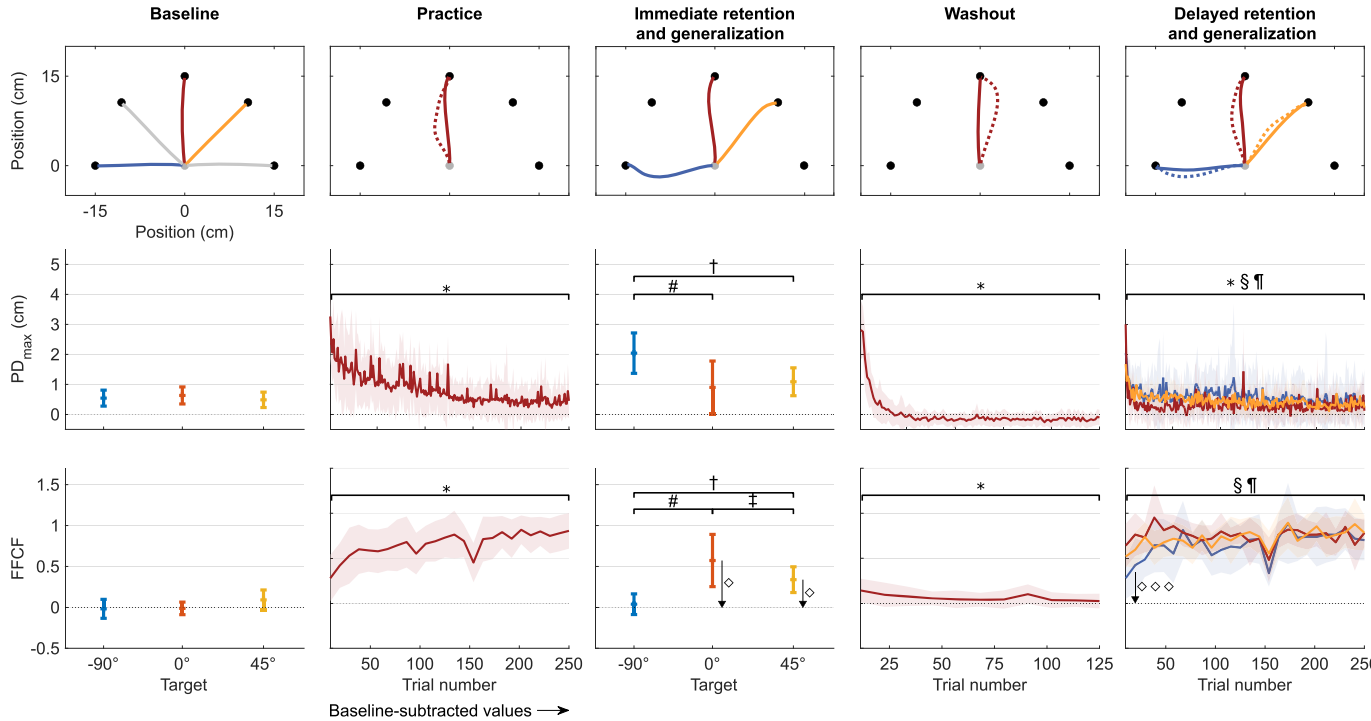

Figure 4. Kinematic and kinetic results. In columns: the different phases are arranged chronologically from *left* to *right*. *Top*: mean trajectories. Solid lines in baseline and immediate retention and generalization are mean values across all NF and FF trials and all participants. Dashed lines in practice, washout, and retention/generalization show mean values across all participants' first two trials in the respective phases. Solid lines, likewise, for the last two trials. *Middle* and *bottom*: PD_{max} and FFCF mean and standard deviation values. *, §, and ¶Statistically significant differences over time for the 0°, −90°, and 45° targets, respectively. #Statistically significant difference between performance for the −90° and 0° target; †between the −90° and the 45°; and ‡between the 0° and 45° target. ◇ Statistically significant different value from zero. FF, force field; FFCF, force field compensation factor; NF, null field.

$t(35) = -9.43$, $P < 0.001$, $d = -2.06$; 0° vs. 45°: $t(35) = 4.01$, $P < 0.001$, $d = 0.91$].

In summary, in the immediate phase, participants showed retention, and also generalized better to the 45° than the −90° target (Fig. 4).

Participants Readapted to the Practiced Direction and Showed Better Generalization to the 45° than to the −90° Target at the Delayed Retention and Generalization Test

After the successful washout and a 10-min break, the participants were randomly assigned to one of the three groups (−90°, 0°, and 45°) and tested whether they adapted (again) and presented differences across the directions.

All groups showed retention or generalization on the first trial as assessed with t tests versus 0 on the FFCF values [−90°: $t(11) = 5.47$, $P < 0.001$, $d = 1.47$; 0°: $t(11) = 13.61$, $P < 0.001$, $d = 3.66$; 45°: $t(11) = 13.83$, $P < 0.001$, $d = 3.71$].

All groups showed a lower PD_{max} value at the end of the delayed retention and generalization phase than at the beginning [0° group: $t(11) = 6.95$, $P < 0.001$, $d = 2.64$; −90° group: $t(11) = 4.73$, $P < 0.001$, $d = 1.80$; 45° group: $t(11) = 7.91$, $P < 0.001$, $d = 3.00$]. The 0° group did not show a higher FFCF value at the end than at the beginning, but the −90° and 45° groups did [0° group: $t(11) = -0.25$, $P = 0.807$, $d = -0.07$; −90° group: $t(11) = -4.66$, $P = 0.001$, $d = -1.63$; 45° group: $t(11) = -4.56$, $P = 0.001$, $d = -1.41$]. To sum up, all participants showed retention or generalization at the beginning. Then, the −90° and 45° groups improved their performances further during the generalization phase, whereas improvement of the 0° group was only apparent in PD_{max}.

We used LMM analysis to assess differences between the groups during the initial phase of retention and generalization [20 trials; ICC = 0.316 (PD_{max}) and 0.333 (FFCF); Table 1]. Based on PD_{max}, the 0° group adapted better than the 45° and −90° groups ($P = 0.004$; $P = 0.038$), whereas the 45° and −90° groups did not adapt differently ($P = 0.937$). Based on FFCF, the groups did not adapt differently ($P = 0.095$; $P = 0.357$; $P = 1.000$), but the 0° group showed a generally better adaptation than the −90° group ($P = 0.001$) and the 45° group a generally better adaptation than the −90° group ($P = 0.004$). Taken together, this indicated that the 0° group (re)adapted best, and the generalization was better for the 45° than for the −90° group, leading us to accept H_{Task} 2.

Movement speed and thus the experienced force field were consistent across participants, directions, and phases (Supplemental Figs. S2 and S3, and Supplemental Table S1).

Two to Five Muscle Synergies Are Used during Baseline

We used muscle synergy analysis to assess the changes in muscle patterns underlying force field adaptation. First, we extracted muscle synergies from the baseline phase. Across all participants, 3.6 ± 0.6 synergies led to a reconstruction quality (R^2) of 0.82 ± 0.04 (Table 2). Figure 5 displays the R^2 for every participant, as well as EMG, synergies, and their reconstruction for one exemplary participant. Across all participants, baseline muscle synergies comprised simultaneous activations of multiple muscles, including monoarticular

Table 1. *Statistical results of the LMM on the first 20 trials of the delayed retention and generalization phases*

	PD_{max}, Reference Group: 0°			FFCF, Reference Group: 0°		
	Estimate (Lower, Upper 95% CI)	*t*	*P*	Estimate (Lower, Upper 95% CI)	*t*	*P*
Fixed effects						
(Intercept)	1.38 (1.13, 1.62)	10.89	<0.001*	0.55 (0.40, 0.70)	7.27	<0.001*
DIR90	0.13 (−0.22, 0.48)	0.74	0.922	−0.37 (−0.58, −0.16)	−3.47	0.001*
DIR45	−0.15 (−0.50, 0.21)	−0.82	0.830	−0.03 (−0.25, 0.18)	−0.32	1.000
TrialNumber	−0.07 (−0.09, −0.06)	−9.01	<0.001*	0.02 (0.01, 0.03)	3.48	0.001*
DIR90_TrialNumber	0.03 (0.00, 0.05)	2.35	0.038*	0.01 (−0.01, 0.02)	0.65	1.000
DIR45_TrialNumber	0.03 (0.01, 0.06)	3.07	0.004*	−0.01 (−0.03, 0.01)	−1.35	0.357
Random effects						
(Intercept)	0.30 (0.22, 0.40)			0.10 (0.06, 0.17)		
Error	0.64 (0.60, 0.68)			0.21 (0.18, 0.23)		
	PD_{max}, Reference Group: −90°			FFCF, Reference Group: −90°		
Fixed effects						
(Intercept)	1.51 (1.26, 1.76)	11.93	<0.001*	0.18 (0.03, 0.33)	2.37	0.038*
DIR0	−0.13 (−0.48, 0.22)	−0.74	0.922	0.37 (0.16, 0.58)	3.47	0.001*
DIR45	−0.28 (−0.63, 0.07)	−1.55	0.242	0.34 (0.13, 0.55)	3.15	0.004*
TrialNumber	−0.04 (−0.06, −0.03)	−5.69	<0.001*	0.03 (0.01, 0.04)	4.40	<0.001*
DIR0_TrialNumber	−0.03 (−0.05, −0.00)	−2.35	0.038*	−0.01 (−0.02, 0.01)	−0.65	1.000
DIR45_TrialNumber	0.01 (−0.01, 0.03)	0.73	0.937	−0.02 (−0.03, −0.00)	−2.00	0.095
Random effects						
(Intercept)	0.30 (0.22, 0.40)			0.10 (0.06, 0.17)		
Error	0.64 (0.60, 0.68)			0.21 (0.18, 0.23)		

PD_{max} values in cm for readability. CI, confidence interval; FFCF, force field compensation factor; LMM, linear mixed model. *Statistical significance after correction for multiple testing.

and biarticular muscles. Five of the eight baseline muscle synergy clusters were directionally tuned according to a cosine tuning function (Fig. 6).

The Muscle Patterns after Adaptation Cannot Be Reconstructed by Baseline Reaching Synergies Only, and Require Adaptation-Specific Muscle Synergies

We tested whether the muscle patterns of force field adaptation can be reconstructed by a combination of baseline reaching synergies ($H_{Synergies}$ *1*). The reconstruction quality R^2 was significantly worse for the adapted state than for the cross-validated R^2_{CV} of the baseline [$t(35) = 7.61$, $P < 0.001$, $d = 1.76$], with R^2 values on average 1.12 ± 0.72 lower for every participant (Table 2). This low reconstruction quality, that is, the mismatch between the reconstructed EMG and the original EMG, is illustrated in the example of Fig. 5*D*. Hence, muscle synergies of unperturbed reaching cannot explain muscle patterns for reaching in a force field, and we reject $H_{Synergies}$ *1*.

Subsequently, we tested whether specific muscle synergies are required using the bootstrap approach ($H_{Synergies}$ *2*). The higher the number of shared synergies, the more subspace dimensions are shared. Across all participants, we found 1.47 ± 0.74 shared synergies but 2.97 ± 0.74 baseline-specific and 1.92 ± 0.60 adapted state-specific synergies. All synergies were clustered across all participants into four shared, seven baseline-specific, and three adapted state-specific synergies clusters (Figs. 7 and 8).

Three of the four shared synergies are directionally tuned, two toward the left and one to the right. Two synergies (*clusters 1* and *4*) show high activation in the middle and end of the adapted state trial and may, therefore, represent a deceleration of the reach. One synergy tuned to the right side is active at the beginning of the adapted state trial, probably to counteract the perturbation. However, the shared synergies do not contribute much to representing adapted state reaching, as an additional 1.92 ± 0.60 adapted state-specific synergies were necessary to describe the muscle pattern in the adapted state.

The baseline-specific synergies and their activation function overall resemble those of the synergies extracted solely from the baseline. The baseline *clusters 1*, *2*, *3*, *4*, *5*, *6*, and *7* from the shared-and-specific extraction resemble baseline *clusters 3* and *4*, *2*, *1*, *5*, *8*, *7*, and *6* from the baseline extraction only (Figs. 6 and 7). Accordingly, the synergies used during the baseline are specific to this phase and are not used in the adapted state.

The adapted state-specific synergy *cluster 1* (Fig. 8) shows high activations of muscles that extend the elbow and the shoulder horizontally, that is, rotate the arm outward while extending it. This synergy is activated early in the movement, with its peak activity shortly after the start. *Cluster 2* shows high activations of TriLat and TriMed, the two main contributors for elbow extension; it is active over the whole trial, with the peak in the middle of the movement. *Cluster 3* shows the coactivation of many muscles that act in opposing directions (e.g., DeltA and DeltM, PectMaj and LatDorsi), probably reflecting cocontraction, and especially high activations of Bic, DeltA and DeltM, and PectMaj. These muscles can be seen as antagonists of the aforementioned muscles during the reaching movement toward the 0° target. This synergy shows two peak activations, the first before the beginning of the movement and the second before reaching the target. The three synergies are activated in four phases. After an initial cocontraction (*cluster 3*), *clusters 1* and *2* are activated, leading to forces toward the target ($Force_y$) and against the counter-clockwise force field ($Force_x$). Interestingly, the two synergies' activations overlap but have their peaks one after the other; yet $Force_x$ has a Gaussian shape without any jitter. Afterward, the

Table 2. *Individual results from the muscle synergy analysis*

Participant	Group	Baseline Synergies	R^2 Baseline	R^2_{CV} Baseline (Means and SD)	R^2 Fit of Baseline Synergies on the Last 4 FF Trials of the Practice Phase	Shared Synergies Baseline and Adapted State	Baseline-Specific Synergies	Adapted State-Specific Synergies	R^2 Fit of Baseline Synergies on the First 4 Retention/ Generalization Trials	R^2 Fit of Shared-and-Specific Synergies on the First 4 Retention/ Generalization Trials	Shared Synergies Baseline and Adapted State and Retention/ Generalization	Retention/ Generalization-Specific Synergies
1	0°	4	0.88	0.75 ± 0.14	−0.90	2	3	2	−2.53	0.53	2	1
2	0°	3	0.75	0.72 ± 0.17	0.31	0	3	2	0.31	0.57	2	1
3	45°	4	0.72	0.71 ± 0.16	−0.40	3	2	1	−0.83	−0.69	3	2
4	−90°	4	0.85	0.73 ± 0.15	0.33	2	3	3	−0.68	−0.36	3	2
5	45°	4	0.81	0.73 ± 0.16	−1.54	1	4	2	0.37	0.43	3	2
6	45°	3	0.81	0.74 ± 0.15	0.51	2	2	2	−0.34	−0.23	3	1
7	45°	3	0.84	0.74 ± 0.13	−1.24	1	3	2	−1.56	−0.71	3	2
8	0°	3	0.79	0.70 ± 0.24	−0.60	1	2	2	−0.19	0.52	3	1
9	0°	3	0.81	0.72 ± 0.15	−0.03	2	2	1	0.01	0.36	3	1
10	−90°	4	0.82	0.73 ± 0.16	−0.52	2	3	1	0.08	0.18	2	2
11	45°	2	0.83	0.75 ± 0.13	−0.92	1	2	2	−1.03	−0.51	2	3
12	0°	4	0.81	0.73 ± 0.17	0.43	2	3	1	0.00	0.26	2	2
13	45°	4	0.87	0.70 ± 0.20	−0.14	1	4	2	−1.03	−0.00	2	2
14	−90°	3	0.81	0.75 ± 0.14	0.20	2	2	2	0.01	0.31	3	2
15	−90°	3	0.79	0.74 ± 0.13	−2.45	0	3	2	−1.11	−0.99	3	2
16	0°	4	0.81	0.71 ± 0.21	−1.39	1	4	3	−0.88	0.24	2	1
17	−90°	3	0.84	0.72 ± 0.19	−0.37	1	3	2	−0.98	−0.65	2	1
18	45°	4	0.79	0.72 ± 0.26	0.09	2	3	1	−0.46	−0.33	3	1
19	−90°	4	0.84	0.69 ± 0.23	0.16	2	3	2	0.53	0.68	3	1
20	−90°	4	0.84	0.73 ± 0.15	−0.09	1	4	3	−1.09	0.26	3	2
21	0°	4	0.81	0.70 ± 0.23	0.52	3	2	2	0.10	0.21	2	1
22	0°	3	0.82	0.69 ± 0.23	−1.03	0	3	2	−1.93	0.19	3	2
23	−90°	5	0.92	0.73 ± 0.15	0.46	1	5	1	−0.68	−0.61	2	2
24	0°	4	0.82	0.72 ± 0.14	−0.15	2	3	2	0.04	0.54	2	2
25	45°	3	0.76	0.75 ± 0.11	−0.40	1	3	2	−0.43	0.00	2	3
26	−90°	3	0.82	0.74 ± 0.15	−1.93	1	3	2	−0.95	0.42	2	2
27	45°	4	0.77	0.73 ± 0.13	−0.30	1	4	3	−1.67	−0.43	3	1
28	0°	3	0.79	0.73 ± 0.16	−1.25	1	3	2	0.17	0.43	2	1
29	0°	3	0.87	0.73 ± 0.17	0.24	1	3	2	−0.36	0.23	2	2
30	45°	3	0.79	0.75 ± 0.11	0.35	2	2	1	−0.58	−0.04	3	2
31	45°	3	0.80	0.73 ± 0.16	0.14	2	2	1	−2.06	−1.52	0	4
32	0°	4	0.85	0.73 ± 0.22	−0.35	2	3	2	−1.20	0.43	3	2
33	−90°	4	0.83	0.75 ± 0.13	−0.97	2	3	2	−0.65	0.52	2	2
34	−90°	4	0.84	0.72 ± 0.18	−0.33	2	3	2	−1.12	−0.48	3	2
35	−90°	4	0.85	0.72 ± 0.16	−0.38	2	3	2	−0.91	−0.35	3	2
36	45°	4	0.83	0.73 ± 0.18	−0.33	1	4	3	−0.80	−0.59	2	1
Means ± SD	0°	3.5 ± 0.5	0.82 ± 0.04	0.72 ± 0.04	−0.35 ± 0.67	1.42 ± 0.09	2.83 ± 0.58	1.92 ± 0.51	−0.54 ± 0.91	0.38 ± 0.14	2.33 ± 0.49	1.42 ± 0.51
Means ± SD	−90°	3.8 ± 0.6	0.84 ± 0.03	0.73 ± 0.03	−0.49 ± 0.89	1.50 ± 0.67	3.17 ± 0.72	2.00 ± 0.60	−0.63 ± 0.45	−0.09 ± 0.55	2.58 ± 0.51	1.83 ± 0.39
Means ± SD	45°	3.4 ± 0.7	0.80 ± 0.04	0.72 ± 0.04	−0.35 ± 0.62	1.50 ± 0.67	2.92 ± 0.90	1.83 ± 0.72	−0.87 ± 0.66	−0.39 ± 0.49	2.42 ± 0.90	2.00 ± 0.95

The *bottom* three rows present the results aggregated for the three groups (−90°, 0°, and 45°).

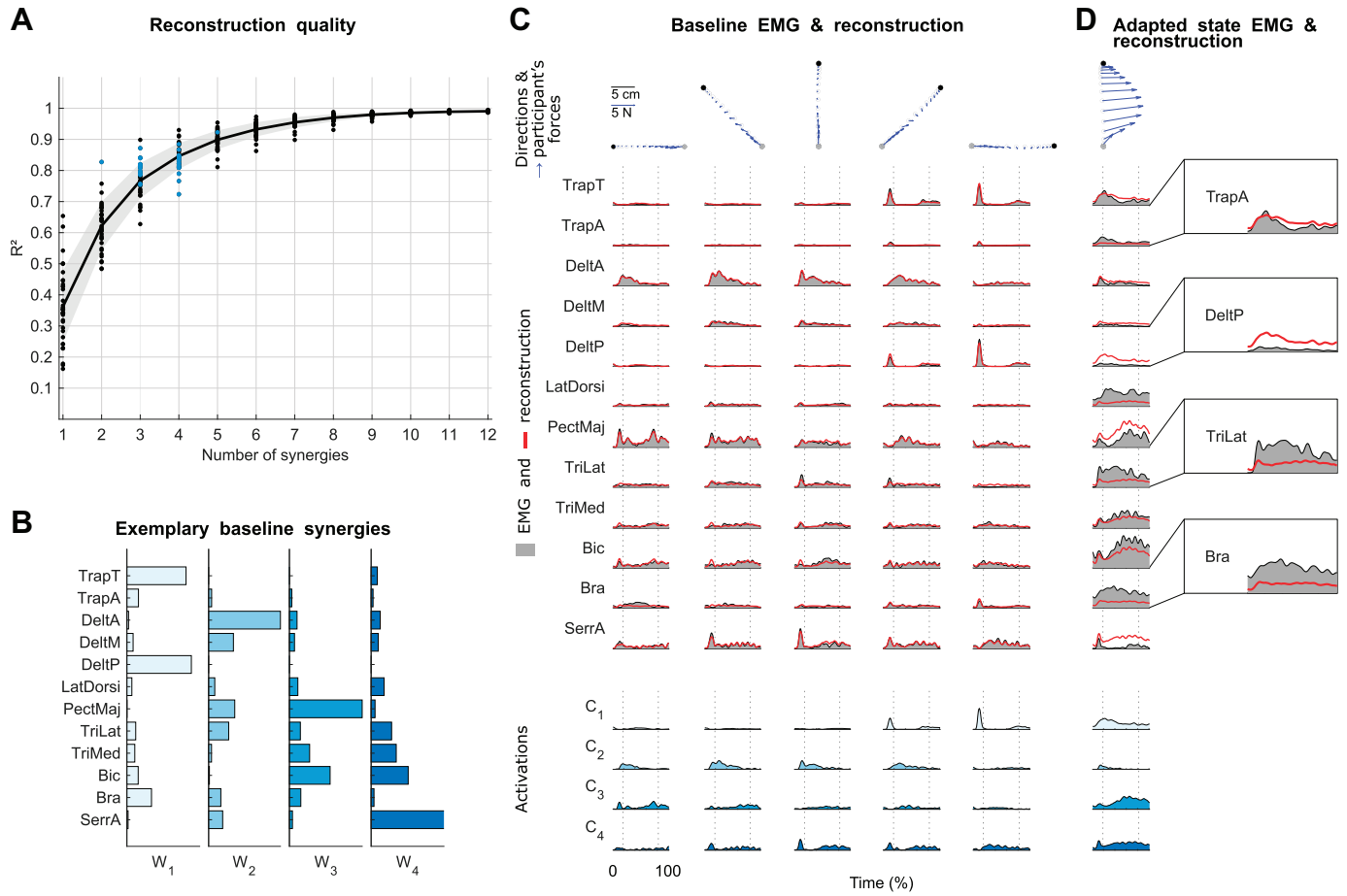

Figure 5. Muscle synergy extraction from baseline. *A*: reconstruction quality R^2 as a function of the number of extracted synergies. The dots represent individual values and the solid, shaded line represents means and standard deviation. Blue colored dots show the participant-specific selected numbers based on the R^2 knee criterion. *B*: baseline muscle synergies extracted from one exemplary participant. *C*, *top*: mean trajectory and forces averaged over all trials for every direction during baseline from the same exemplary participant. The distances of the dots illustrating the trajectories display the reaching speed (interdot distance corresponds to 8% of the trial duration). *C*, *middle*: EMG averaged over all trials for each direction during baseline from the same exemplary participant (gray) and the respective reconstructions (red). *C*, *bottom*: activation functions for every direction in columns. Each activation function belongs to one muscle synergy (e.g., C_1 belongs to W_1). *D*: trajectories, forces, and EMG averaged over the last 20 FF trials during adaptation for the same participant and the respective reconstruction by the baseline synergies ("baseline fit"). The enlargements show the mismatches in detail for four muscles. The dotted lines in *C* and *D* show the time points when the participant left the start point and reached the target point. Bic, biceps brachii; Bra, brachioradialis; DeltA, deltoid anterior; DeltM, deltoid middle; DeltP, deltoid posterior; EMG, electromyogram; FF, force field; LatDorsi, latissimus dorsi; PectMaj, pectoralis major; SerrA, serratus anterior; TrapA, trapezius ascending; TrapT, trapezius transverse; TriLat, triceps brachii lateralis; TriMed, triceps brachii medialis.

arm is decelerated by *cluster 3*, which is reflected in the negative values of Force_y.

The reconstruction quality $R^2_{\text{W-POOL}\rightarrow\text{Adapted state}}$ was significantly lower than $R^2_{\text{W-SAS}\rightarrow\text{Adapted state}}$ [$R^2_{\text{W-POOL}\rightarrow\text{Adapted state}} = 0.62 \pm 0.15$, $R^2_{\text{W-SAS}\rightarrow\text{Adapted state}} = 0.71 \pm 0.15$; $t(35) = -8.63$, $P < 0.05$, $d = -1.44$). This affirms the finding that force field adaptation requires adapted state-specific muscle synergies, rather than a larger set including both baseline and adapted state-specific muscle synergies.

Figure 9 shows the detailed reconstruction of the adapted state for the exemplary participant with the shared-and-specific synergy extraction. One synergy is shared between the baseline and the adapted state (Fig. 9*B*, W1), as obtained by evaluating the principal angle distributions (Fig. 9*C*). There are four baseline-specific synergies (W2–W5), resembling those of the baseline-only extraction (Fig. 5), except that the high PectMaj activity is now present in the shared synergy W1. Most interestingly, the adapted state-specific synergies W6 and W7 show the subsequent but overlapping activation of two synergies that reflect arm extension and outward rotation, probably leading to forces necessary for adapted reaching. This stands in contrast with unperturbed reaching. Although one synergy (W5) showed agonistic muscle activations for unperturbed 0° reaching, two muscle synergies showed it in the adapted state reaching (W6 and W7). One specialty of this participant is the high activation of the Bic throughout the movement.

In summary, the adapted state EMG patterns are represented predominantly by adapted state-specific muscle synergies with a four-phasic activation pattern.

Muscle Synergies Acquired during Adaptation Facilitate Delayed Retention and Generalization

Kinematics and kinetics indicated that the 0° group showed retention and that the 45° and 90° groups showed generalization, with slightly better values for the 45° group

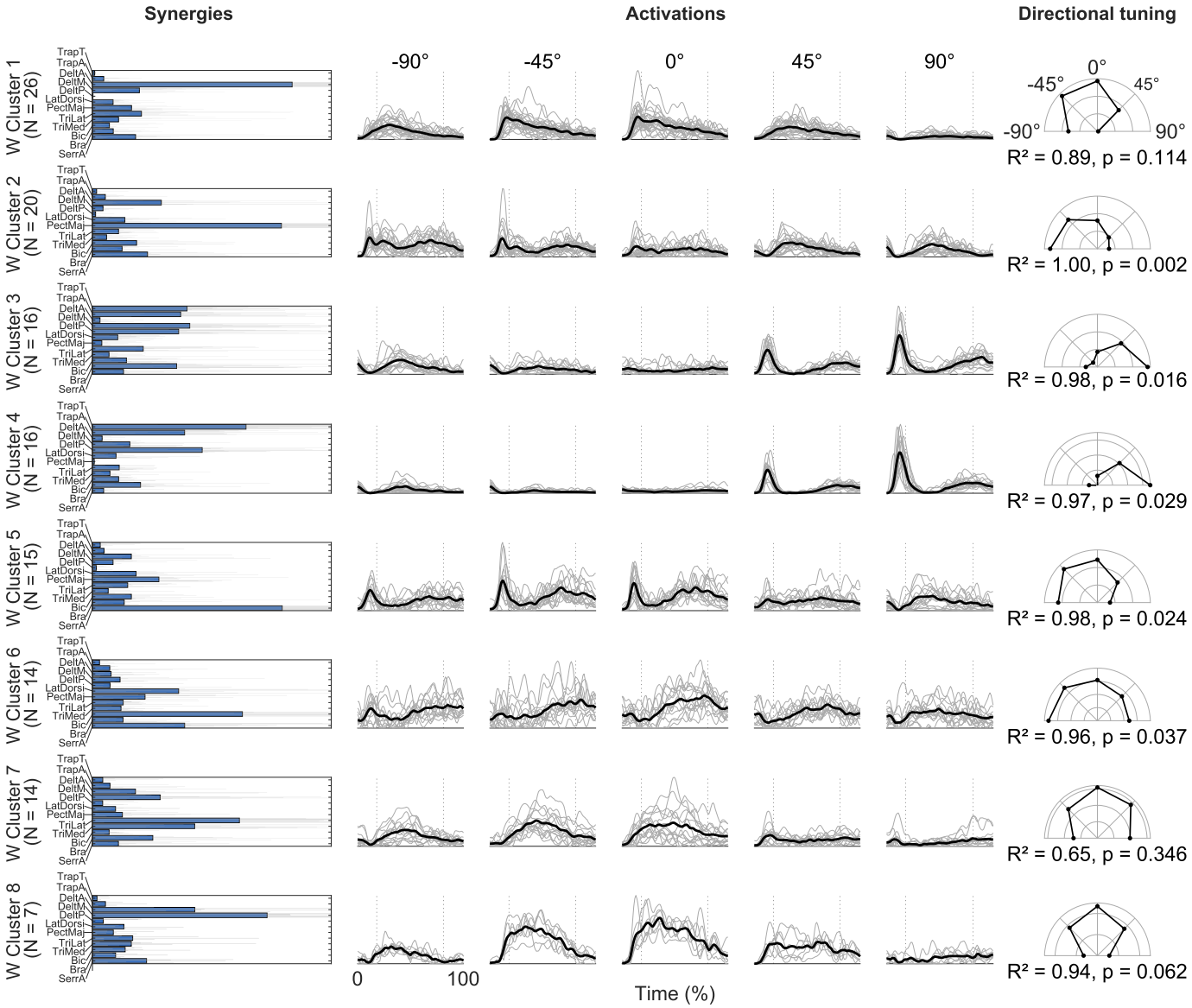

Figure 6. Clustering and cosine fit of the baseline synergies. The *left* column shows the centroids (filled bars) and the individual synergies in gray solid lines. The *middle* column shows the mean (black, solid lines) and the individual (gray, solid lines) activation functions separated for the five directions. The dotted lines show the average time points when the participants left the start point and reached the target point. The *right* column shows the cosine tuning. Bic, biceps brachii; Bra, brachioradialis; DeltA, deltoid anterior; DeltM, deltoid middle; DeltP, deltoid posterior; LatDorsi, latissimus dorsi; PectMaj, pectoralis major; SerrA, serratus anterior; TrapA, trapezius ascending; TrapT, trapezius transverse; TriLat, triceps brachii lateralis; TriMed, triceps brachii medialis.

(*Participants Readapted to the Practiced Direction and Showed Better Generalization to the 45° than to the −90° Target at the Delayed Retention and Generalization Test*). Therefore, we tested whether muscle synergies can reflect these findings using the shared-and-specific synergies extracted from the baseline and adapted state to reconstruct the muscle patterns of the delayed generalization phase ($H_{Synergies}$ *3*).

We found that the shared-and-specific synergies explained the muscle patterns at the beginning (first four FF trials) of the delayed retention and generalization phase better than the baseline synergies, as all groups showed a significant improvement in the reconstruction quality R^2 ($-90°$: $W = 78$, $P < 0.001$, $d = 1.02$; $0°$: $W = 78$, $P < 0.001$, $d = 0.93$; $45°$: $W = 78$, $P < 0.001$, $d = 1.16$; Table 2, Fig. 10*A*). Figure 10*A* further shows that the difference is greater than zero, with very few exceptions, over the whole delayed retention and generalization phase. This means that the muscle patterns of the delayed retention and generalization phase can be better explained by the synergies that capture the changes occurring during adaptation (shared-and-specific synergies) than those that do not (baseline synergies). However, there was no difference between the groups regarding the improvement in reconstruction achieved with shared-and-specific synergies with respect to baseline synergies on the first four FF trials [$H(2, 35) = 1.76$, $P = 0.415$, $\eta^2 = 0.05$].

Next, we investigated the dimensionality and the structure of the muscle synergies that facilitate retention

and generalization. This was done by comparing the shared-and-specific synergies extracted from the baseline and adapted state together and the synergies extracted from retention/generalization trials. We found 2.50 ± 0.50 shared dimensions between the subspaces spanned by the baseline and adapted state synergies and retention/generalization synergies. Hence, more synergies are shared in this case than between baseline and adapted state

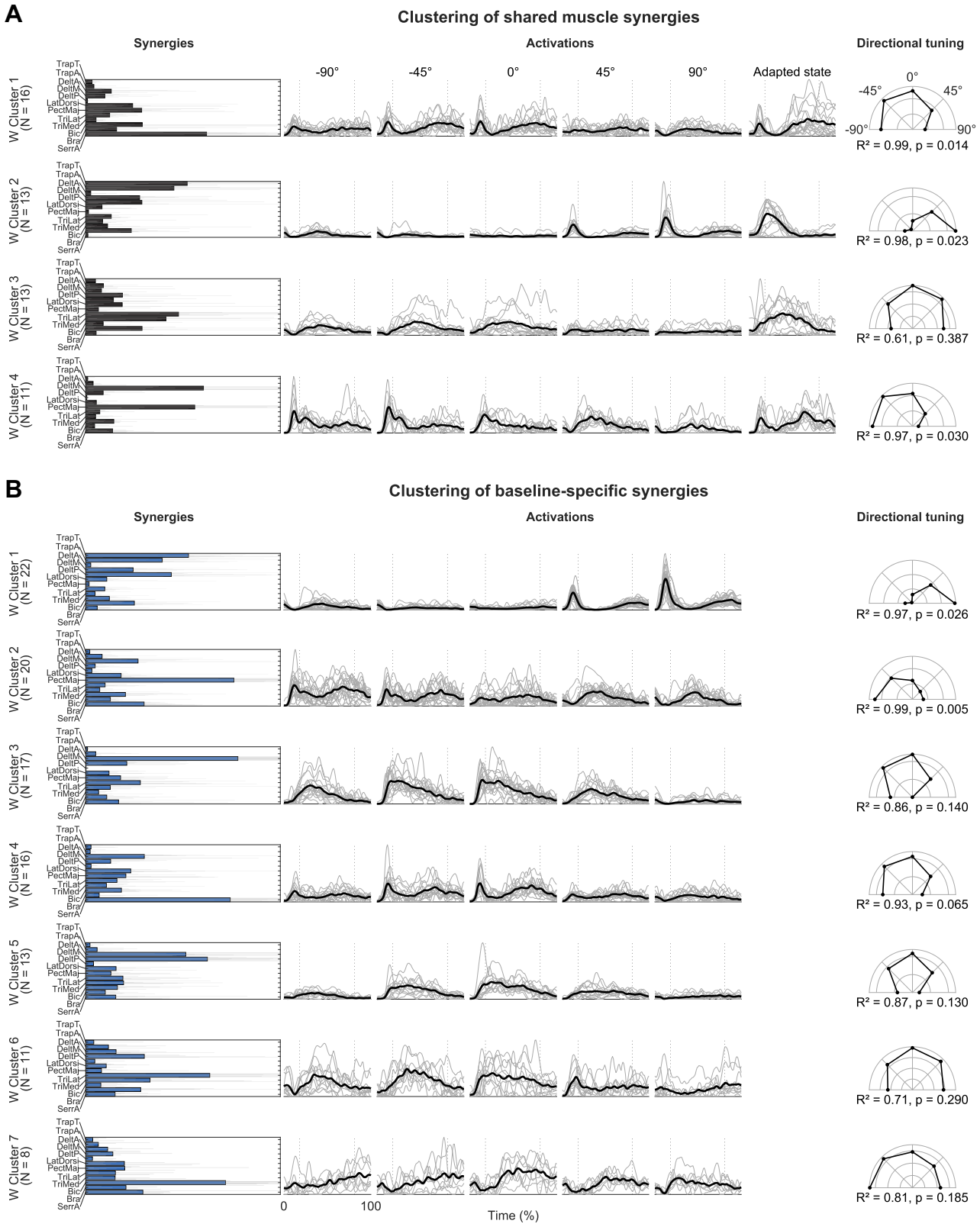

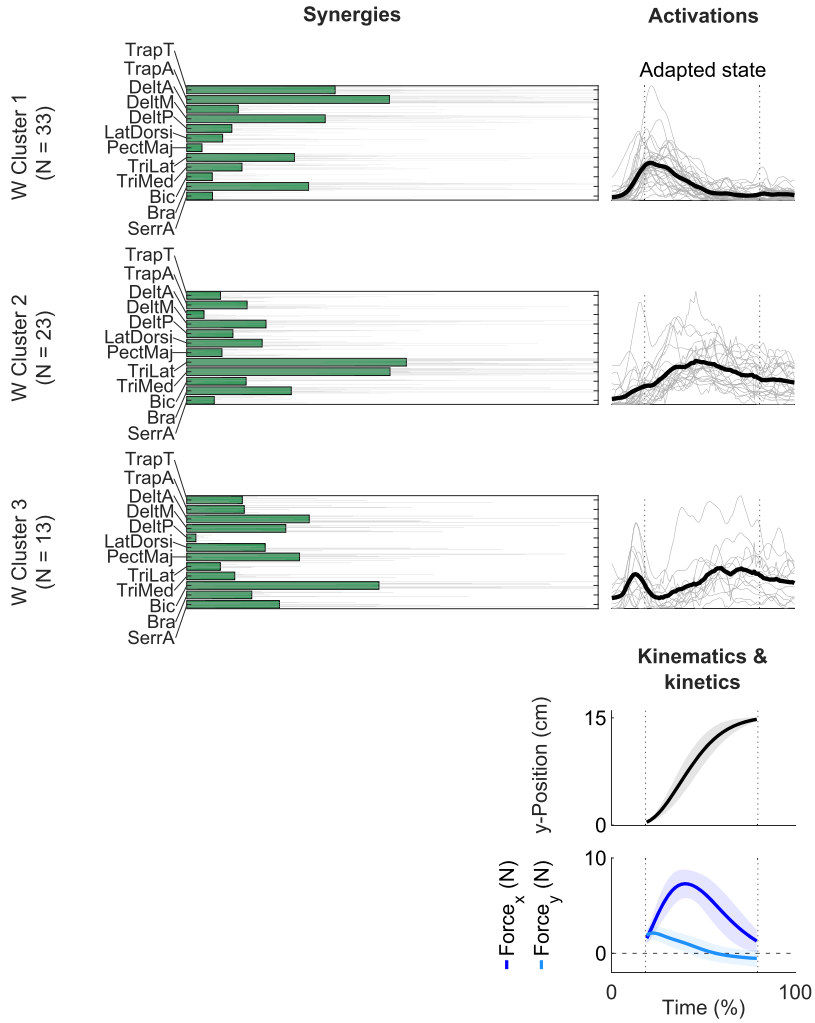

Figure 8. Shared-and-specific synergy extraction and clustering of the adapted state-specific synergies. The *left* column shows the centroid (filled bars) and the individual synergies in gray solid lines. The *right* column shows the mean (black, solid lines) and the individual (gray, solid lines) activation functions. Below, the position of the handle in the *y*-direction is shown as means (solid black line) and standard deviation (gray shaded) across all participants and the last 20 FF trials. Similarly, the participant's mean forces in the *x*- and *y*-directions are shown as means (blue solid lines) and standard deviations (blue shaded line). The dotted lines show the average time points when the participants left the start point and reached the end point. The dashed line shows 0 N. Bic, biceps brachii; Bra, brachioradialis; DeltA, deltoid anterior; DeltM, deltoid middle; DeltP, deltoid posterior; FF, force field; LatDorsi, latissimus dorsi; PectMaj, pectoralis major; SerrA, serratus anterior; TrapA, trapezius ascending; TrapT, trapezius transverse; TriLat, triceps brachii lateralis; TriMed, triceps brachii medialis.

synergies (Fig. 10*B*). Accordingly, the higher number of shared dimensions indicates that the muscle synergies reflect the findings of retention and generalization in the kinematic and kinetic variables. The acquired structural changes in the synergies that occurred during adaptation may facilitate delayed retention and generalization. Figure 10*C* shows the clusters of the shared synergies between the baseline and adapted state synergies and the retention/generalization synergies. The first three resemble the adapted state-specific synergies reported in *The Muscle Patterns after Adaptation Cannot Be Reconstructed by Baseline Reaching Synergies Only, and Require Adaptation-Specific Muscle Synergies* (*clusters 1*, *2*, and *3* in Fig. 10*C* resemble *clusters 2*, *3*, and *1* in Fig. 8). Furthermore, for the retention, we observe the described four-phasic pattern again. Moreover, the 45° group shows a similar four-phasic pattern, with the same synergies activated one after another, as the 0° retention group. The −90° group differs from the 0° and 45° groups. *Cluster 1* is activated later in the movement and *cluster 2* is activated earlier, probably accelerating the arm toward the target instead of decelerating, and only two participants show synergies for *cluster 3*. Still, we observe that two muscle synergies are activated in an overlapping manner with subsequent activity peaks when the handle moves between the start and stop targets, just as the 0° and 45° groups.

However, the differences between the groups observed with PD_{max} and FFCF are not well reflected in the modular structure, as we found no differences regarding the reconstruction quality of the baseline and adapted state shared-and-specific synergies on the first four retention/generalization FF trials or the number of specific synergies between the −90° and the 45° groups. Hence, we reject $H_{Synergies}$ 3.

Figure 7. Results of the clustering of the shared-and-specific muscle synergy extraction of baseline and adapted state. *A*: clusters of the shared muscle synergies. *B*: clusters of the baseline-specific muscle synergies. The *left* column shows the centroids (filled bars) and the individual synergies in gray solid lines. The *middle* column shows the mean (black, solid lines) and the individual (gray, solid lines) activation functions. The dotted lines show the average time points when the participants left the start point and reached the end point. The *right* column shows the cosine tuning based on the baseline activation functions. Bic, biceps brachii; Bra, brachioradialis; DeltA, deltoid anterior; DeltM, deltoid middle; DeltP, deltoid posterior; LatDorsi, latissimus dorsi; PectMaj, pectoralis major; SerrA, serratus anterior; TrapA, trapezius ascending; TrapT, trapezius transverse; TriLat, triceps brachii lateralis; TriMed, triceps brachii medialis.

DISCUSSION

This study investigated the relationship between muscle synergies and force field adaptation, retention, and generalization. Our findings show that adaptation involves structural changes in muscle synergies compared with reaching in unperturbed conditions, alongside a novel four-phasic synergy activation pattern. Moreover, these

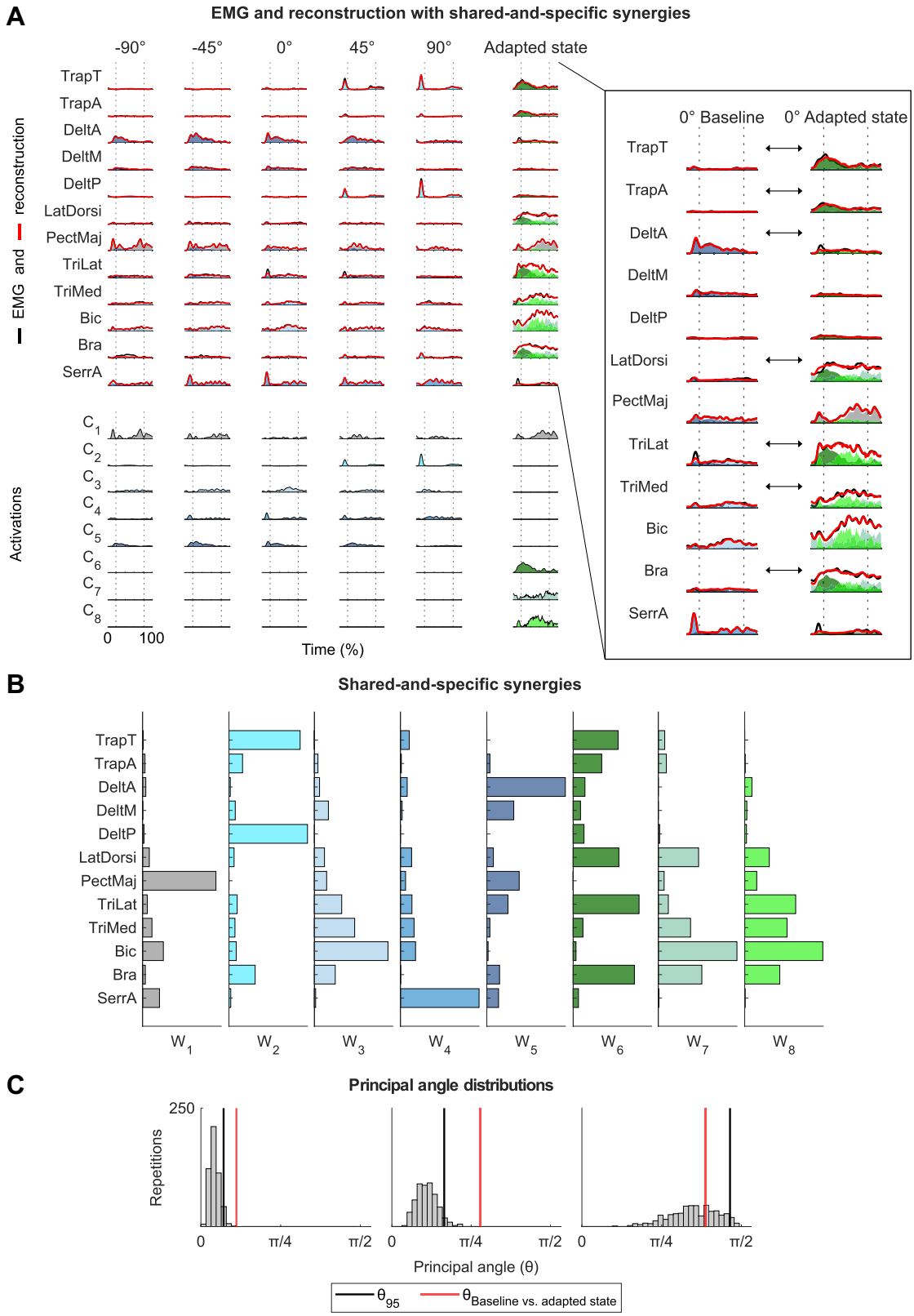

structural changes and activation patterns likely facilitate retention and generalization, as the same synergies and their activation patterns are also reflected there.

Participants Adapted to the Force Field, Showed Retention to the 0° Target, and Generalization to the 45° and −90° Targets

Participants adapted to the force field during their first exposure, washed out after its removal, and readapted and generalized when reexposed (H_{Task} *1*). Moreover, we found that generalization decreased with distance from the practiced movement direction (H_{Task} *2*). These results align with related force field studies (1–3, 7, 65). The fast readaptation for the 0°, that is, the same direction as during the first exposure, has been previously described as the "savings" effect (2, 65, 66). However, based on the aforementioned studies, we expected no generalization to the −90° target at the beginning of the delayed retention and generalization phase. This disagreement may stem from participants already being exposed to the −90° FF condition during the immediate retention and generalization test, as adaptation starts from the very first trial (67). The adaptation, washout, savings, and generalization we identified allowed us to examine the underlying modular structure of the muscle patterns.

Reaching in an Environment with Altered Dynamics Requires Structural Changes to the Muscle Synergies for Unperturbed Reaching

We first extracted muscle synergies from the planar, center-out reaching movements in the null field during the baseline. The number, composition, and tuning of the extracted baseline synergies are in accordance with the literature (43, 68).

Since a possible mechanism for reaching in a force field could be to combine the synergies used in the baseline, we hypothesized that the muscle patterns of force field adaptation can be reconstructed by a combination of baseline reaching synergies ($H_{Synergies}$ *1*). However, our results indicate this is not the case, and force field adaptation requires structural changes in muscle synergies ($H_{Synergies}$ *2*). We found adapted state-specific synergies activated in a four-phasic pattern. First, a synergy reflecting cocontraction is active. Then, there is an early onset of a synergy reflecting arm extension and outward rotation, which is active until halfway through the trial until a second synergy overtakes, mainly reflecting triceps activity and, thus, elbow extension. At the trial end, the movement is decelerated and stabilized through a synergy of antagonistic muscles.

Reaching movements have been found to follow a triphasic pattern of muscle activation, leading to acceleration, deceleration, and damping of the movement (69–71). This pattern is generally also reflected in the activation of muscle synergies, showing an interplay between agonistic and antagonistic muscle synergies (43, 72). These observations regarding EMG and muscle synergies hold for baseline reaching in our study. Moreover, when adapted, participants used a triphasic pattern of muscle activity as previously described (29, 73). However, the novelty of our findings is that the muscle activity used to move the hand to the target is realized through two synergies with overlapping activations, peaking sequentially. Interestingly, the transition between the two synergies is seamless, as the force curves are bell-shaped and smooth. We provide a novel characterization of changes in the synergistic organization of many muscles after adaptation to a perturbing force field. Nevertheless, our findings align with literature examining activities in a few muscles, when looking at the muscle activity in our study without looking at the muscle synergies. We also observed early activity in these muscles, probably reflecting cocontraction (28, 73), and the muscles for reaching forward and counteracting the force field are already active early in the movement (29, 30).

Huang et al. (31) showed that muscle activity is reduced to minimal levels even after a plateau in kinematic- and kinetic-dependent variables. Accordingly, the CNS might optimize effort while adapting, which leads to specific muscle synergies. The synergy that reflects arm extension with high triceps activation is sparse, and may reflect this tendency to realize movements with less effort. However, there is a lack of clarity over the process of how the structural changes happen, that is, whether adaptation-specific synergies separate from the subspaces spanned by baseline synergies by learning new synergies, or whether adapted state-specific subspaces are the result of other control processes not requiring new synergies. This unmet need motivates future studies.

Force field adaptation with a muscle synergy perspective has received little research attention. Oscari et al. (26) found that moving a joystick in a viscous force field involves two additional muscle synergies during adaptation. This supports the notion of structural changes during force field adaptation, even though their results may be limited. Sampling a single direction may limit the validity of extracted synergies (74), characterizing only acceleration and deceleration patterns (72) and neglecting the versatile use of baseline reaching synergies to different directions. In contrast to our findings, a structural change in muscle synergies has not previously been reported during isometric visuomotor rotations (23–25). Here, muscle synergies extracted from the baseline could reconstruct the muscle

Figure 9. Reconstruction of the baseline and adapted state EMG with the shared-and-specific muscle synergies. *A*: EMG (solid black lines) and reconstruction (solid red lines) of the shared-and-specific synergy extraction of one exemplary participant. The reconstruction is calculated as the sum of the products of the synergies with their respective activation functions. Here, the reconstruction of each product is plotted transparently to illustrate its contributions to the overall reconstruction. The activation functions of the synergies are plotted at the *bottom*. The enlargement shows the reconstruction of the 0° baseline and adapted state in greater detail; arrows guide the reader to substantial differences in synergy activations. *B*: muscle synergies. The shared synergy is gray, the baseline-specific synergies in blue shades, and the adapted state-specific synergies in green shades. *C*: combined principal angle distributions obtained with the bootstrapping procedure for the exemplary participant. The vertical black line signifies each distribution's 95th percentile (θ_{95}), and the red line is the principal angle between the baseline and adapted state synergies. Bic, biceps brachii; Bra, brachioradialis; DeltA, deltoid anterior; DeltM, deltoid middle; DeltP, deltoid posterior; EMG, electromyogram; LatDorsi, latissimus dorsi; PectMaj, pectoralis major; SerrA, serratus anterior; TrapA, trapezius ascending; TrapT, trapezius transverse; TriLat, triceps brachii lateralis; TriMed, triceps brachii medialis.

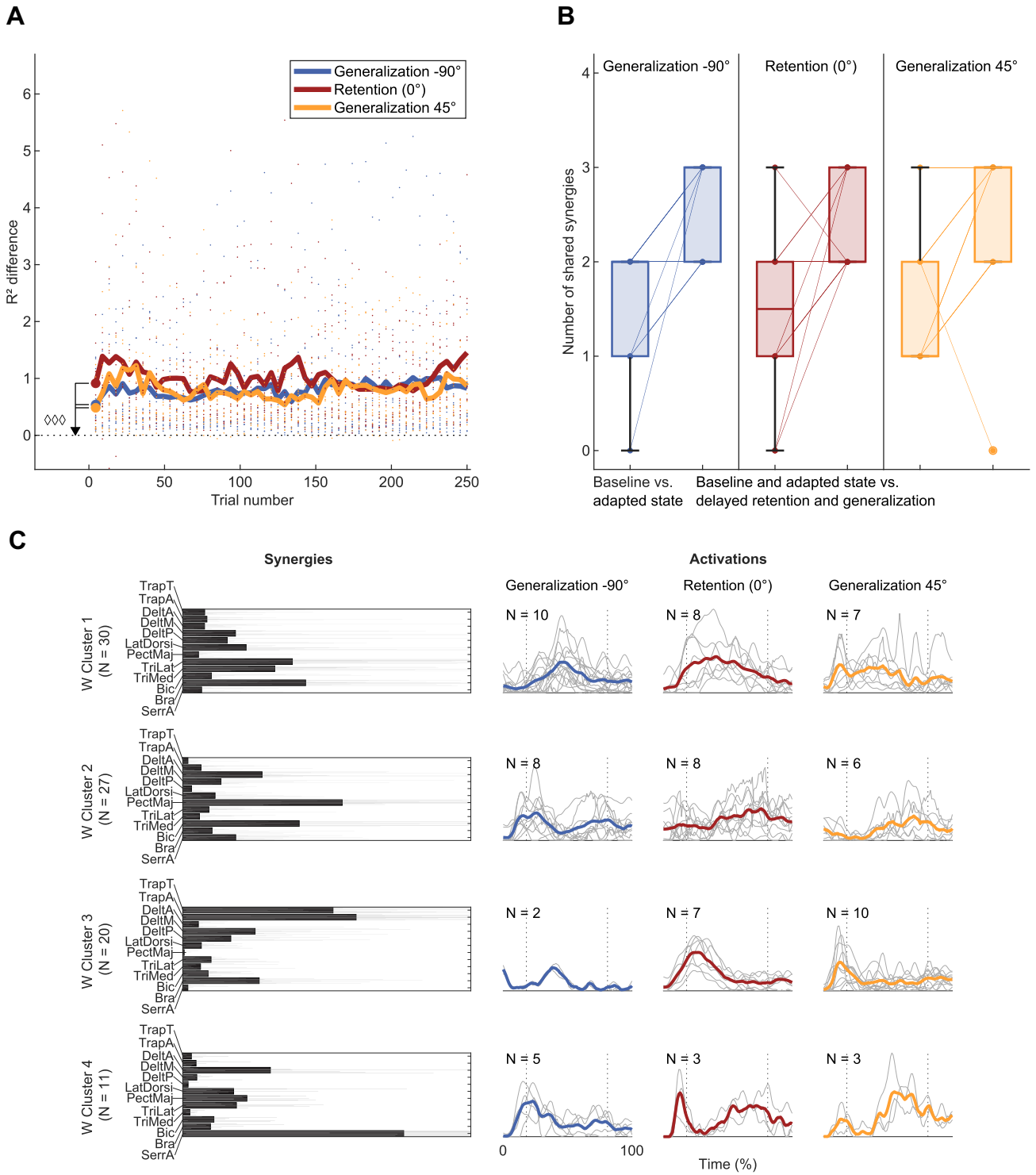

Figure 10. *A*: difference in reconstruction quality (R^2) between fitting of shared-and-specific and baseline synergies on blocks of delayed retention/generalization trials, which were averaged over four FF trials. The thick lines represent the mean and dots represent individual values. The values are presented according to their group. A value larger than zero indicates that shared-and-specific synergies better reconstructed the EMG retention/generalization trials than baseline synergies. The three ♢ symbols indicate significant differences from zero for all groups for the averaged first four FF trials (thick dots). *B*: comparison of how many synergies are shared between *1*) the baseline and the adapted state and *2*) the shared-and-specific synergies of the baseline and adapted state together and the first 20 delayed retention/generalization trials. The box chart shows the median and the lower and upper quartiles, and lines show individual values. *C*: clustering results of the shared synergies from the shared-and-specific synergy extraction of baseline and adapted state together and the first 20 retention/generalization trials. The *left* column shows the centroid (filled bars) and the individual synergies in gray solid lines. The *right* columns show the mean (solid lines) and the individual (gray, solid lines) activation functions, separated for the three groups. The dotted lines show the average time points when the participants left the start point and reached the target point. Bic, biceps brachii; Bra, brachioradialis; DeltA, deltoid anterior; DeltM, deltoid middle; DeltP, deltoid posterior; EMG, electromyogram; FF, force field; LatDorsi, latissimus dorsi; PectMaj, pectoralis major; SerrA, serratus anterior; TrapA, trapezius ascending; TrapT, trapezius transverse; TriLat, triceps brachii lateralis; TriMed, triceps brachii medialis.

patterns during adaptation and generalization, indicating structural robustness. Although force field and visuomotor adaptation are related motor adaptation paradigms, there are some differences (75), especially when the latter is done under isometric conditions. In isometric conditions, the force exerted on the handle by the participant is realized through muscle activations while the joint configurations remain. This stands in contrast with dynamic reaching in a force field. In the latter, the joint angles and muscle lengths change throughout the movement, and the force exerted by the participant on the handle depends on the joint angle, muscle length, and their derivatives (17, 20, 76, 77). Furthermore, in visuomotor rotation, the imposed perturbation is consistent with respect to the perturbation-cursor location relation. This further stays in contrast with force field adaptation, in which the perturbing force is dependent on the handle's velocity and thus not consistent throughout the reach, as reaching is typically performed with a Gaussian-like velocity profile (78). These differences may explain why a tuning of baseline muscle synergies, to realize a rotation of the forces exerted by the participant to facilitate visuomotor rotation adaptation, was insufficient in force field adaptation ($H_{Synergies\ 1}$ rejected). In contrast, we propose that force field adaptation requires muscle synergies to be appropriate and effort-optimized at all joint angle configurations used during the reach. In this regard, future studies could further disentangle isometric and nonisometric adaptation paradigms, for example, compare force field adaptation and visuomotor rotation in nonisometric conditions.

This study's findings of structural changes can also be discussed with those found with incompatible virtual surgeries (79). In the latter paradigm, tendons of muscles are virtually swapped by a modification of the muscle-to-force relationship. This altered mapping requires participants to change the muscle synergy structure to eventually fulfil the reaching task, as a change in the muscle synergy tuning would not suffice, just as in our study. Still, although participants adapt within one session in force field adaptation, they achieve it only after an extensive exploration phase or multiple sessions after an incompatible surgery, if at all (80). Although a structural change has been related more to skill learning, the structural changes observed in this study, along with related findings in a recent study on exoskeleton walking adaptation in stroke survivors (81), challenge this strict categorization and motivate further study of coordination at a muscular level in motor learning.

Retention and Generalization Are Represented in the Modular Structure after Adaptation

We found that retention and generalization muscle patterns can be better explained with synergies extracted from both baseline and adaptation than from baseline synergies alone. Therefore, the structural changes acquired during adaptation are reused during retention and generalization. The retention (0° target) muscle pattern is well described by the shared synergies. Hence, our results show that muscle synergies and their activation timing are reused when reexposed to the same force field, presumably allowing a fast readaptation. This suggests that the shared muscle synergies represent a mechanism capturing the savings effect at a modular level (2, 65, 66).

However, contrary to our hypothesis $H_{Synergies}$ *3*, the different amount of generalization between the −90° and 45° directions is not evident in the reconstruction quality, the number of shared synergies, or the number of direction-specific synergies. Accordingly, the structural changes in muscle synergies through adaptation reflect retention and generalization but not the differences between the 0°, −90°, and 45° groups. Possibly, the different adaptation progressions for the three targets (H_{Task} *2*) may result from different levels of difficulty the CNS has to tune the shared-and-specific synergies for the respective direction, such that it might be easier to tune them to the 45° target than the −90° target. The observed structural changes through adaptation probably represent a general, that is, direction-invariant, coordinative solution to the force field perturbation. This supports the notion that muscle synergies represent low-dimensional, modular control, and are reused in reaching to multiple directions (43), yet motivates future studies to further investigate the relationship between muscle coordination and task-level generalization performances. For example, future studies may investigate the trial-by-trial changes separately for the −90° and 45° directions to investigate possible mechanisms related to different generalization speeds. Presumably, although the retention and generalization within the first 20 trials of the delayed retention and generalization phase seem to be facilitated by tuning the shared-and-specific muscle synergies, further adaptation progression (until plateauing of PD_{max} and FFCF at the end) may require further muscle synergy adjustments.

Limitations

Baseline reaching directions comprised a semi-circle, and only center-out movements were analyzed. This restricts the possible subspaces and, thus, potentially shared subspace dimensions with the adapted state. Moreover, all participants adapted to the 0° target first, generalization was assessed with three directions, and only a counter-clockwise force field was used. Accordingly, future studies may generalize our findings with different directions and other force field types. All participants were males, future studies may therefore verify our findings with other sexes. Clipping negative values to zero after removing the tonic parts in the EMG omitted data potentially relatable to the neural underlying of muscle synergies, especially the aspect of inhibitory spinal premotor interneurons (82–84). Due to the limited number of movements, we cannot conclusively state whether the CNS acquired new synergies during adaptation, or whether these synergies are stored in the CNS but were not recruited in the baseline. Furthermore, future studies may investigate how the structural changes in muscle synergies evolve with practice. Although the majority of participants exhibited two or three shared and one or two adaptation-specific synergies, there were a few exceptions. Future studies could investigate whether individual adaptation, saving, or generalization progressions are related to the individual's synergy repertoire and its flexibility.

Conclusions

This study found that reaching in an environment with altered dynamics requires structural changes and novel activation patterns in muscle synergies. These structural changes facilitate retention when readapting to the same direction and generalization when adapting to new directions. Thus, our results provide new insights into how force field adaptation, retention, and spatial generalization are represented at the level of muscular coordination.

DATA AVAILABILITY

Data can be made available upon reasonable request to the authors.

SUPPLEMENTAL MATERIAL

Supplemental Figs. S1–S3 and Supplemental Table S1: https://doi.org/10.5281/zenodo.17170752.

ACKNOWLEDGMENTS

Preprint is available at https://doi.org/10.1101/2024.12.16.628548.

DISCLOSURES

No conflicts of interest, financial or otherwise, are declared by the authors.

AUTHOR CONTRIBUTIONS

M.H. and T.S. conceived and designed research; M.H. performed experiments; M.H. analyzed data; M.H., D.J.B., M.R., A.D., and T.S. interpreted results of experiments; M.H. prepared figures; M.H. drafted manuscript; M.H., D.J.B., M.R., A.D., and T.S. edited and revised manuscript; M.H., D.J.B., M.R., A.D., and T.S. approved final version of manuscript.

REFERENCES

1. **Shadmehr R**, **Mussa-Ivaldi FA.** Adaptive representation of dynamics during learning of a motor task. *J Neurosci* 14: 3208–3224, 1994. doi:10.1523/JNEUROSCI.14-05-03208.1994.
2. **Brashers-Krug T**, **Shadmehr R**, **Bizzi E.** Consolidation in human motor memory. *Nature* 382: 252–255, 1996. doi:10.1038/382252a0.
3. **Gandolfo F**, **Mussa-Ivaldi FA**, **Bizzi E.** Motor learning by field approximation. *Proc Natl Acad Sci USA* 93: 3843–3846, 1996. doi:10.1073/pnas.93.9.3843.
4. **Ghez C**, **Krakauer JW**, **Sainburg R**, **Ghilardi M.** Spatial representations and internal models of limb dynamics in motor learning. In: *The Cognitive Neurosciences*, edited by Gazzaniga M**.** The MIT Press, 1999, p. 501–514.
5. **Shadmehr R.** Generalization as a behavioral window to the neural mechanisms of learning internal models. *Hum Mov Sci* 23: 543–568, 2004. doi:10.1016/j.humov.2004.04.003.
6. **Shadmehr R.** Learning to predict and control the physics of our movements. *J Neurosci* 37: 1663–1671, 2017. doi:10.1523/JNEUROSCI.1675-16.2016.
7. **Rezazadeh A**, **Berniker M.** Force field generalization and the internal representation of motor learning. *PLoS One* 14: e0225002, 2019 [Erratum in *PLoS One* 15: e0227963, 2020]. doi:10.1371/journal.pone.0225002.
8. **Diedrichsen J**, **White O**, **Newman D**, **Lally N.** Use-dependent and error-based learning of motor behaviors. *J Neurosci* 30: 5159–5166, 2010. doi:10.1523/JNEUROSCI.5406-09.2010.
9. **Krakauer JW**, **Mazzoni P.** Human sensorimotor learning: adaptation, skill, and beyond. *Curr Opin Neurobiol* 21: 636–644, 2011. doi:10.1016/j.conb.2011.06.012.
10. **Thoroughman KA**, **Shadmehr R.** Learning of action through adaptive combination of motor primitives. *Nature* 407: 742–747, 2000. doi:10.1038/35037588.
11. **Wolpert DM**, **Kawato M.** Multiple paired forward and inverse models for motor control. *Neural Netw* 11: 1317–1329, 1998. doi:10.1016/S0893-6080(98)00066-5.
12. **d'Avella A.** Modularity for Motor Control and Motor Learning. In: *Progress in Motor Control: Theories and Translations*, edited by Laczko J, Latash ML**.** Springer International Publishing, 2016, p. 3–19.
13. **Bernstein NA.** *The Co-Ordination and Regulation of Movements*. Pergamon Press, 1967.
14. **Bizzi E**, **Cheung VCK**, **d'Avella A**, **Saltiel P**, **Tresch M.** Combining modules for movement. *Brain Res Rev* 57: 125–133, 2008. doi:10.1016/j.brainresrev.2007.08.004.
15. **Giszter SF.** Motor primitives—new data and future questions. *Curr Opin Neurobiol* 33: 156–165, 2015. doi:10.1016/j.conb.2015.04.004.
16. **Mussa-Ivaldi FA.** Modular features of motor control and learning. *Curr Opin Neurobiol* 9: 713–717, 1999. doi:10.1016/S0959-4388(99)00029-X.
17. **Bizzi E**, **Mussa-Ivaldi FA**, **Giszter S.** Computations underlying the execution of movement: a biological perspective. *Science* 253: 287–291, 1991. doi:10.1126/science.1857964.
18. **Tresch MC**, **Saltiel P**, **Bizzi E.** The construction of movement by the spinal cord. *Nat Neurosci* 2: 162–167, 1999. doi:10.1038/5721.
19. **d'Avella A**, **Saltiel P**, **Bizzi E.** Combinations of muscle synergies in the construction of a natural motor behavior. *Nat Neurosci* 6: 300–308, 2003. doi:10.1038/nn1010.
20. **Mussa-Ivaldi FA**, **Giszter SF**, **Bizzi E.** Linear combinations of primitives in vertebrate motor control. *Proc Natl Acad Sci USA* 91: 7534–7538, 1994. doi:10.1073/pnas.91.16.7534.
21. **Mussa–Ivaldi FA**, **Bizzi E.** Motor learning through the combination of primitives. *Phil Trans R Soc Lond B* 355: 1755–1769, 2000. doi:10.1098/rstb.2000.0733.
22. **Ting LH**, **Macpherson JM.** A limited set of muscle synergies for force control during a postural task. *J Neurophysiol* 93: 609–613, 2005. doi:10.1152/jn.00681.2004.
23. **De Marchis C**, **Di Somma J**, **Zych M**, **Conforto S**, **Severini G.** Consistent visuomotor adaptations and generalizations can be achieved through different rotations of robust motor modules. *Sci Rep* 8: 12657, 2018. doi:10.1038/s41598-018-31174-2.
24. **Gentner R**, **Edmunds T**, **Pai DK**, **d'Avella A.** Robustness of muscle synergies during visuomotor adaptation. *Front Comput Neurosci* 7: 120, 2013. doi:10.3389/fncom.2013.00120.
25. **Severini G**, **Zych M.** Characterization of the adaptation to visuomotor rotations in the muscle synergies space. *Front Bioeng Biotechnol* 8: 605, 2020. doi:10.3389/fbioe.2020.00605.
26. **Oscari F**, **Finetto C**, **Kautz SA**, **Rosati G.** Changes in muscle coordination patterns induced by exposure to a viscous force field. *J Neuroeng Rehabil* 13: 58, 2016. doi:10.1186/s12984-016-0164-3.
27. **Franklin S**, **Franklin DW.** Feedback gains modulate with motor memory uncertainty. *Neurons behav data anal theory* 5: 1–28, 2021. doi:10.51628/001c.22336.
28. **Milner T**, **Franklin DW.** Impedance control and internal model use during the initial stage of adaptation to novel dynamics in humans. *J Physiol* 567: 651–664, 2005. doi:10.1113/jphysiol.2005.090449.
29. **Thoroughman KA**, **Shadmehr R.** Electromyographic correlates of learning an internal model of reaching movements. *J Neurosci* 19: 8573–8588, 1999. doi:10.1523/JNEUROSCI.19-19-08573.1999.
30. **Albert ST**, **Shadmehr R.** The neural feedback response to error as a teaching signal for the motor learning system. *J Neurosci* 36: 4832–4845, 2016. doi:10.1523/JNEUROSCI.0159-16.2016.
31. **Huang HJ**, **Kram R**, **Ahmed AA.** Reduction of metabolic cost during motor learning of arm reaching dynamics. *J Neurosci* 32: 2182–2190, 2012. doi:10.1523/JNEUROSCI.4003-11.2012.
32. **Franklin DW**, **Osu R**, **Burdet E**, **Kawato M**, **Milner TE.** Adaptation to stable and unstable dynamics achieved by combined impedance control and inverse dynamics model. *J Neurophysiol* 90: 3270–3282, 2003. doi:10.1152/jn.01112.2002.
33. **Oldfield RC.** The assessment and analysis of handedness: the Edinburgh inventory. *Neuropsychologia* 9: 97–113, 1971. doi:10.1016/0028-3932(71)90067-4.
34. **Joiner WM**, **Smith MA.** Long-term retention explained by a model of short-term learning in the adaptive control of reaching. *J Neurophysiol* 100: 2948–2955, 2008. doi:10.1152/jn.90706.2008.

35. **Scheidt RA**, **Reinkensmeyer DJ**, **Conditt MA**, **Rymer WZ**, **Mussa-Ivaldi FA.** Persistence of motor adaptation during constrained, multi-joint, arm movements. *J Neurophysiol* 84: 853–862, 2000. doi:10.1152/jn.2000.84.2.853.
36. **Hermens HJ**, **Freriks B**, **Disselhorst-Klug C**, **Rau G.** Development of recommendations for SEMG sensors and sensor placement procedures. *J Electromyogr Kinesiol* 10: 361–374, 2000. doi:10.1016/S1050-6411(00)00027-4.
37. **Perotto AO.** *Anatomical Guide for the Electromyographer: The Limbs and Trunk* (5th ed). Charles C Thomas Publisher, 2011.
38. **Herzog M**, **Focke A**, **Maurus P**, **Thürer B**, **Stein T.** Random practice enhances retention and spatial transfer in force field adaptation. *Front Hum Neurosci* 16: 816197, 2022. doi:10.3389/fnhum.2022.816197.
39. **Stockinger C**, **Thürer B**, **Focke A**, **Stein T.** Intermanual transfer characteristics of dynamic learning: direction, coordinate frame, and consolidation of interlimb generalization. *J Neurophysiol* 114: 3166–3176, 2015. doi:10.1152/jn.00727.2015.
40. **Peri E**, **Xu L**, **Ciccarelli C**, **Vandenbussche NL**, **Xu H**, **Long X**, **Overeem S**, **van Dijk JP**, **Mischi M.** Singular value decomposition for removal of cardiac interference from trunk electromyogram. *Sensors (Basel)* 21: 573, 2021. doi:10.3390/s21020573.
41. **Ahmad I**, **Ansari F**, **Dey UK.** Power line noise reduction in ECG by Butterworth notch filters: a comparative study. *IJECIERD* 3: 65–74, 2013.
42. **Anwar MN**, **Tomi N**, **Ito K.** Motor imagery facilitates force field learning. *Brain Res* 1395: 21–29, 2011. doi:10.1016/j.brainres.2011.04.030.
43. **d'Avella A**, **Portone A**, **Fernandes L**, **Lacquaniti F.** Control of fast-reaching movements by muscle synergy combinations. *J Neurosci* 26: 7791–7810, 2006. doi:10.1523/JNEUROSCI.0830-06.2006.
44. **Heald JB**, **Franklin DW**, **Wolpert DM.** Increasing muscle co-contraction speeds up internal model acquisition during dynamic motor learning. *Sci Rep* 8: 16355, 2018. doi:10.1038/s41598-018-34737-5.
45. **Sing GC**, **Joiner WM**, **Nanayakkara T**, **Brayanov JB**, **Smith MA.** Primitives for motor adaptation reflect correlated neural tuning to position and velocity. *Neuron* 64: 575–589, 2009. doi:10.1016/j.neuron.2009.10.001.
46. **Wagner MJ**, **Smith MA.** Shared internal models for feedforward and feedback control. *J Neurosci* 28: 10663–10673, 2008. doi:10.1523/JNEUROSCI.5479-07.2008.
47. **Cheung VCK**, **d'Avella A**, **Tresch MC**, **Bizzi E.** Central and sensory contributions to the activation and organization of muscle synergies during natural motor behaviors. *J Neurosci* 25: 6419–6434, 2005. doi:10.1523/JNEUROSCI.4904-04.2005.
48. **Cheung VCK**, **d'Avella A**, **Bizzi E.** Adjustments of motor pattern for load compensation via modulated activations of muscle synergies during natural behaviors. *J Neurophysiol* 101: 1235–1257, 2009. doi:10.1152/jn.01387.2007.
49. **d'Avella A**, **Bizzi E.** Shared and specific muscle synergies in natural motor behaviors. *PNAS* 102: 3076–3081, 2005. doi:10.1073/pnas.0500199102.
50. **Lee DD**, **Seung HS.** Learning the parts of objects by non-negative matrix factorization. *Nature* 401: 788–791, 1999. doi:10.1038/44565.
51. **Lee DD**, **Seung HS.** Algorithms for non-negative matrix factorization. In: *Advances in Neural Information Processing Systems 13*, edited by Leen TK, Dietterich TG, Tresp V**.** The MIT Press, 2001, p. 556–562.
52. **Russo M**, **Scano A**, **Brambilla C**, **d'Avella A.** SynergyAnalyzer: a Matlab toolbox implementing mixed-matrix factorization to identify kinematic-muscular synergies. *Comput Methods Programs Biomed* 251: 108217, 2024. doi:10.1016/j.cmpb.2024.108217.
53. **Bach MM**, **Daffertshofer A**, **Dominici N.** Muscle synergies in children walking and running on a treadmill. *Front Hum Neurosci* 15: 637157, 2021. doi:10.3389/fnhum.2021.637157.
54. **Carey HD**, **Liss DJ**, **Allen JL.** Young adults recruit similar motor modules across walking, turning, and chair transfers. *Physiol Rep* 9: e15050, 2021. doi:10.14814/phy2.15050.
55. **Stone M.** Cross-validatory choice and assessment of statistical predictions. *J R Stat Soc Ser B Stat Methodol* 36: 111–133, 1974. doi:10.1111/j.2517-6161.1974.tb00994.x.
56. **Brambilla C**, **Russo M**, **d'Avella A**, **Scano A.** Phasic and tonic muscle synergies are different in number, structure and sparseness. *Hum Mov Sci* 92: 103148, 2023. doi:10.1016/j.humov.2023.103148.
57. **Sylos-Labini F**, **La Scaleia V**, **Cappellini G**, **Fabiano A**, **Picone S**, **Keshishian ES**, **Zhvansky DS**, **Paolillo P**, **Solopova IA**, **d'Avella A**, **Ivanenko Y**, **Lacquaniti F.** Distinct locomotor precursors in newborn babies. *Proc Natl Acad Sci USA* 117: 9604–9612, 2020. doi:10.1073/pnas.1920984117.
58. **Golub GH**, **Van Loan CF.** *Matrix Computations* (2nd ed.). Johns Hopkins University Press, 1989.
59. **Allen JL**, **Kesar TM**, **Ting LH.** Motor module generalization across balance and walking is impaired after stroke. *J Neurophysiol* 122: 277–289, 2019. doi:10.1152/jn.00561.2018.
60. **Ippersiel P**, **Preuss R**, **Fillion A**, **Jean-Louis J**, **Woodrow R**, **Zhang Q**, **Robbins SM.** Inter-joint coordination and the flexion-relaxation phenomenon among adults with low back pain during bending. *Gait Posture* 85: 164–170, 2021. doi:10.1016/j.gaitpost.2021.02.001.
61. **Russell DM**, **Haworth JL.** Walking at the preferred stride frequency maximizes local dynamic stability of knee motion. *J Biomech* 47: 102–108, 2014. doi:10.1016/j.jbiomech.2013.10.012.
62. **Hox J**, **Moerbeek M**, **van de Schoot R.** *Multilevel Analysis: Techniques and Applications* (3rd ed.). Routledge, 2017.
63. **Holm S.** A simple sequentially rejective multiple test procedure. *Scand J Stat* 6: 65–70, 1979.
64. **Cohen J.** *Statistical Power for the Behavioural Sciences* (2nd ed.). Lawrence Erlbaum Associates, 1988.
65. **Mathew J**, **Lefèvre P**, **Crevecoeur F.** Savings in human force field learning supported by feedback adaptation. *eNeuro* 8: ENEURO.0088-21.2021, 2021. doi:10.1523/ENEURO.0088-21.2021.
66. **Shadmehr R**, **Brashers-Krug T.** Functional stages in the formation of human long-term motor memory. *J Neurosci* 17: 409–419, 1997. doi:10.1523/JNEUROSCI.17-01-00409.1997.
67. **Joiner WM**, **Sing GC**, **Smith MA.** Temporal specificity of the initial adaptive response in motor adaptation. *PLoS Comput Biol* 13: e1005438, 2017. doi:10.1371/journal.pcbi.1005438.
68. **Muceli S**, **Boye AT**, **d'Avella A**, **Farina D.** Identifying representative synergy matrices for describing muscular activation patterns during multidirectional reaching in the horizontal plane. *J Neurophysiol* 103: 1532–1542, 2010. doi:10.1152/jn.00559.2009.
69. **Flanders M**, **Pellegrini JJ**, **Soechting JF.** Spatial/temporal characteristics of a motor pattern for reaching. *J Neurophysiol* 71: 811–813, 1994. doi:10.1152/jn.1994.71.2.811.
70. **Happee R.** Goal-directed arm movements: I. Analysis of EMG records in shoulder and elbow muscles. *J Electromyogr Kinesiol* 2: 165–178, 1992. doi:10.1016/1050-6411(92)90014-A.
71. **Wadman WJ**, **van der Gon JJD**, **Geuze RH**, **Mol CR.** Control of fast goal-directed arm movements. *J Hum Mov Stud* 5: 3–17, 1979.
72. **Chiovetto E**, **Berret B**, **Delis I**, **Panzeri S**, **Pozzo T.** Investigating reduction of dimensionality during single-joint elbow movements: a case study on muscle synergies. *Front Comput Neurosci* 7: 11, 2013. doi:10.3389/fncom.2013.00011.
73. **Darainy M**, **Ostry DJ.** Muscle cocontraction following dynamics learning. *Exp Brain Res* 190: 153–163, 2008. doi:10.1007/s00221-008-1457-y.
74. **Steele KM**, **Tresch MC**, **Perreault EJ.** Consequences of biomechanically constrained tasks in the design and interpretation of synergy analyses. *J Neurophysiol* 113: 2102–2113, 2015. doi:10.1152/jn.00769.2013.
75. **Krakauer JW**, **Ghilardi M-F**, **Ghez C.** Independent learning of internal models for kinematic and dynamic control of reaching. *Nat Neurosci* 2: 1026–1031, 1999. doi:10.1038/14826.
76. **Giszter SF**, **Mussa-Ivaldi FA**, **Bizzi E.** Convergent force fields organized in the frog's spinal cord. *J Neurosci* 13: 467–491, 1993. doi:10.1523/JNEUROSCI.13-02-00467.1993.
77. **Shadmehr R**, **Wise SP.** *The Computational Neurobiology of Reaching and Pointing: A Foundation for Motor Learning*. The MIT Press, 2005.
78. **Morasso P.** Spatial control of arm movements. *Exp Brain Res* 42: 223–227, 1981. doi:10.1007/BF00236911.
79. **Berger DJ**, **Gentner R**, **Edmunds T**, **Pai DK**, **d'Avella A.** Differences in adaptation rates after virtual surgeries provide direct evidence for modularity. *J Neurosci* 33: 12384–12394, 2013. doi:10.1523/JNEUROSCI.0122-13.2013.
80. **Berger DJ**, **Borzelli D**, **d'Avella A.** Task space exploration improves adaptation after incompatible virtual surgeries. *J Neurophysiol* 127: 1127–1146, 2022. doi:10.1152/jn.00356.2021.

81. **Rinaldi L**, **Yeung L-F**, **Lam PC-H**, **Pang MYC**, **Tong RK-Y**, **Cheung VCK.** Adapting to the mechanical properties and active force of an exoskeleton by altering muscle synergies in chronic stroke survivors. *IEEE Trans Neural Syst Rehabil Eng* 28: 2203–2213, 2020. doi:10.1109/TNSRE.2020.3017128.
82. **Cheung VCK**, **Seki K.** Approaches to revealing the neural basis of muscle synergies: a review and a critique. *J Neurophysiol* 125: 1580–1597, 2021. doi:10.1152/jn.00625.2019.
83. **Guo X**, **Huang S**, **He B**, **Lan C**, **Xie JJ**, **Lau KYS**, **Takei T**, **Mak ADP**, **Cheung RTH**, **Seki K**, **Cheung VCK**, **Chan RHM.** Inhibitory components in muscle synergies factorized by the rectified latent variable model from electromyographic data. *IEEE J Biomed Health Inform* 29: 1049–1061, 2025. doi:10.1109/JBHI.2024.3453603.
84. **Takei T**, **Confais J**, **Tomatsu S**, **Oya T**, **Seki K.** Neural basis for hand muscle synergies in the primate spinal cord. *Proc Natl Acad Sci USA* 114: 8643–8648, 2017. doi:10.1073/pnas.1704328114.